Acta Pharmaceutica Sinica B 2026;16(6):3934−3952

Chinese Pharmaceutical Association
Institute of Materia Medica, Chinese Academy of Medical Sciences

Acta Pharmaceutica Sinica B

www.elsevier.com/locate/apsb
www.sciencedirect.com

ORIGINAL ARTICLE

Astragalus-derived nano-agonist potentiates chemotherapy by reducing tumor-suppressive macrophages

Xuan Han[a,b,*,†], Yongbing Yang[c,†], Qiwen Lu[a], Zihan Zhang[a], Chengcheng Zhang[d], Xi Wang[e], Yueyi Huang[a], Hurong Shen[a], Qichen Zhan[b,g], Jing Chen[b,f,*], Peng Cao[b,d,g,*]

[a]*School of Integrated Medicine, Nanjing University of Chinese Medicine, Nanjing 210023, China*
[b]*State Key Laboratory of Technologies for Chinese Medicine Pharmaceutical Process Control and Intelligent Manufacture, Nanjing University of Chinese Medicine, Nanjing 210023, China*
[c]*Interdisciplinary Eye Research Institute (EYE-X Institute), Bengbu Medical University, Bengbu 233030, China*
[d]*Jiangsu Provincial Integrated Innovation Center of Hospital Preparations, Affiliated Hospital of Integrated Traditional Chinese and Western Medicine, Nanjing University of Chinese Medicine, Nanjing 210023, China*
[e]*The First Clinical Medical College, Nanjing University of Chinese Medicine, Nanjing 210023, China*
[f]*School of Pharmacy, Nanjing University of Chinese Medicine, Nanjing 210023, China*
[g]*Jiangsu Key Laboratory for Pharmacology and Safety Research of Chinese Materia Medica, School of Pharmacy, Nanjing University of Chinese Medicine, Nanjing 210023, China*

Received 17 May 2025; received in revised form 9 June 2025; accepted 13 June 2025

KEY WORDS

Breast cancer;
Chemotherapy;
Formononetin;
Immunotherapy;
Macrophage;
Myelosuppression;
Nanoparticle;
Toll-like receptors 2

Abstract Platinum-based chemotherapy only achieves a short-term success in the treatment of triple-negative breast cancer (TNBC), which is attributed to immunosuppressive macrophages post-chemotherapy. Herein, inspired by the plant immune defense mechanism, we demonstrate that edible astragalus-derived exosome-like nanoparticles (ADNPs) exhibit conspicuous efficacy in reprogramming M1-like tumor-associated macrophages (TAMs) through the activation of TLR2 signaling. The docking between released formononetin and TLR2 plays a key role during the cell internalization process. As a result, ADNPs in combination with Cisplatin (termed ADNP-Cis) greatly inhibit TNBC murine tumor progression and metastasis. Besides, ADNPs alleviate the peripheral blood toxicity caused by cisplatin

*Corresponding authors.
E-mail addresses: hanxuan@njucm.edu.cn (Xuan Han), jingchen3236@njucm.edu.cn (Jing Chen), cao_peng@njucm.edu.cn (Peng Cao).
[†]These authors made equal contributions to this work.

Peer review under the responsibility of Chinese Pharmaceutical Association and Institute of Materia Medica, Chinese Academy of Medical Sciences.

https://doi.org/10.1016/j.apsb.2026.03.051

treatment, and show lower toxicity compared with other TLR2 agonists previously reported. Taken together, this safe and robust ADNP-Cis therapy offers fresh insights into the management of TNBC chemotherapy.

1. Introduction

Triple-negative breast cancer (TNBC) is the most aggressive subtype of breast cancer, accounting for approximately 10%−15% of all newly diagnosed breast cancer cases[1]. Compared to other breast cancer subtypes, TNBC is associated with a poorer prognosis, with higher mortality rates as high as 40% within the first 5 years after diagnosis, and a higher recurrence rate within 1−3 years[2]. Additionally, TNBC is highly invasive; approximately 33% of TNBC patients develop distant metastasis, resulting in a lower median overall survival of only 13−18 months[3]. Given the lack of definitive biomarkers in TNBC, targeted therapy for patients with TNBC remains largely unexplored[4].

Neoadjuvant therapy is initially applied as a preoperative systemic therapy in patients with malignant tumours, including multiple therapies such as endocrine therapy, chemotherapy, and targeted therapy. The role of neoadjuvant therapy has been extensively researched, highlighting its importance in decreasing metastatic foci and enhancing the feasibility of surgical intervention in patients with advanced cancers[5]. Research has demonstrated that neoadjuvant therapy effectively prolongs disease-free survival (DFS) among patients with rectal cancer[6]. A meta-analysis has revealed that 65% of patients who underwent neoadjuvant therapy were able to qualify for breast-conserving surgery. This rate was significantly elevated compared to those who received adjuvant therapy alone[7]. However, the outcome of neoadjuvant therapy remains suboptimal, primarily due to its low efficacy and high toxicity. More than half of patients failed to achieve a pathological complete remission (pCR) after neoadjuvant therapy[8]. Furthermore, patients undergoing neoadjuvant therapy frequently experience chemotherapy-associated adverse effects, including myelosuppression, anaemia, peripheral neuropathy, and nephrotoxicity[9], which can complicate or delay subsequent treatment plans. Accumulated research has indicated that the suboptimal efficacy of neoadjuvant therapy is intimately linked to the immunosuppressive tumour microenvironment (TME) in TNBC[10,11]. A new, safe neoadjuvant therapy, combining chemotherapy and TME restoration, remains in high demand.

The TME primarily consists of various immune cells, for example, tumour-associated macrophages (TAMs), B-lymphocytes, T-lymphocytes, and dendritic cells (DCs)[12]. TAMs account for 10%−20% proportion of TME, highlighting the crucial role in orchestrating anti-tumour immune responses[13]. In the face of different stimuli, TAMs can differentiate into M1-or M2-like phenotypes. M1-like TAMs promote pro-inflammatory response through producing elevated concentrations of pro-inflammatory cytokines, such as TNF-α, IL-12, and promoting $CD8^+$ T-cell activation[14,15]. Conversely, M2-like TAMs promote an anti-inflammatory and pro-tumorigenic phenotype by producing anti-inflammatory cytokines such as TGF-β and IL-10. These cytokines suppress the immune response, promote angiogenesis, and enhance tumour proliferation and invasiveness[16], which contribute to poor patient prognosis[17,18]. TLR agonists have been developed and applied in preclinical and clinical treatment in macrophage polarization. For instance, specific microbial components, particularly pathogen-associated molecular patterns (PAMPs) derived from fungi and bacteria, can efficiently activate toll-like receptors (TLRs) expressed on macrophages, thereby inducing their differentiation into a robust M1-like phenotype[19,20]. However, the PAMPs mimicking TLR agonists have shown insufficient biocompatibility[21], leading to a failure in achieving significant success in clinics. On the other hand, Plants synthesize small RNAs and package them into extracellular vesicles (EVs) to suppress fungal pathogen infections[22,23]. These fresh plant-derived nanoparticles (PDNPs), rather than PAMP analogues, were proven to be novel and efficient nano-agonists that drive the innate immunity of plants. However, little is known about cross-species application of PDNPs in cancer immunotherapy, especially when it is combined with neoadjuvant therapy. Previously, our team found that ginseng-derived exosome-like nanoparticles (GDNPs) could efficiently reverse TAMs polarization and synergize with immunotherapy; however, it remains modest efficacy in the TNBC tumor model[24,25]. Given that the haematological toxicity happened in most patients under chemotherapy, largely limiting the combinable effects with immunotherapy or targeted therapy, it is still highly warranted to explore alternative anti-tumour PDNPs with both high efficiency and low toxicity.

Astragalus has been applied in clinical treatment and food supplements in Asia for thousands of years. Several studies have demonstrated the potential anti-tumour effects and immune remodelling of Astragalus. For instance, astragaloside IV, the active component of Astragalus, has been shown to improve the inflammatory state of endothelial cells in enteritis, reducing the risk of intestinal cancer[26]. Astragalus polysaccharides can effectively enhance the immune activity of TAMs in TNBC, contributing to anti-tumour immune responses[27,28]. Compared to dried Astragalus, fresh Astragalus retains more pharmacologically active components, such as higher levels of *n*-hexanol and *o*-xylene[29]. Astragalus-derived exosome-like nanoparticles (ADNPs) are isolated and purified from the fresh root of *Astragalus membranaceus*. ADNPs have shown vigorous immunity against *Aeromonas hydrophila* infection in tilapia[30]. However, the impact of ADNPs in tumour immunity remains inconclusive.

In this research, inspired by the plant immune defense mechanism, we developed natural ADNPs with encouraging anti-tumorigenic effects *in vivo*. The component of ADNPs, formononetin, can reprogram TAMs efficiently, promote the activation of $CD8^+$ T lymphocytes, and reduce $CD8^+$ T cell exhaustion, thereby enhancing the anti-neoplastic efficacy of cisplatin-based chemotherapy (Fig. 1). Moreover, combining ADNPs with cisplatin-based neoadjuvant therapy (ADNP-Cis) significantly suppresses tumor metastasis and establishes long-term (over 60 days) anti-tumor immune memory in a triple-negative breast cancer (TNBC) murine model. Furthermore, ADNP-Cis therapy

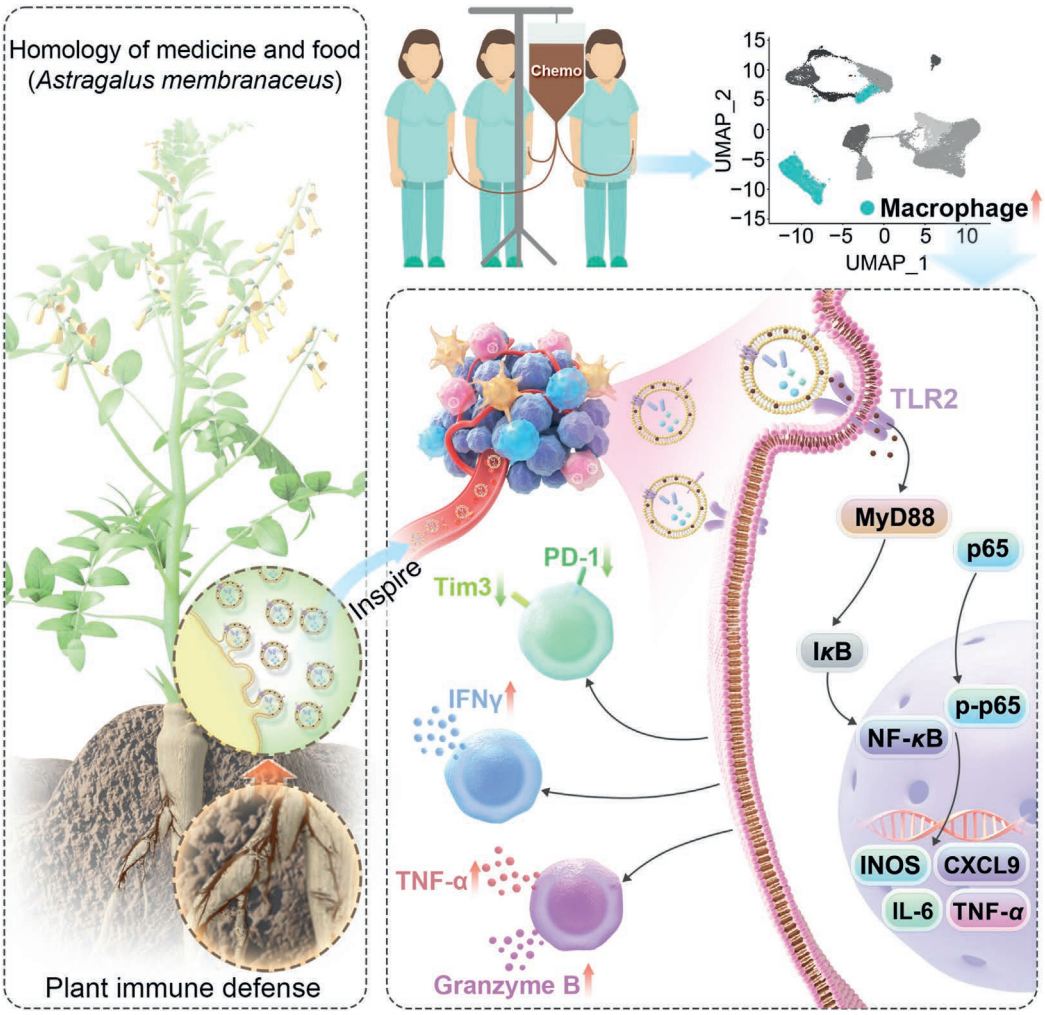

Figure 1 Schematic representation of naturally derived ADNPs polarizing TAMs, enhancing chemotherapy in TNBCs.

improves cisplatin-induced myelosuppression by increasing red blood cell counts. Together, ADNP-Cis therapy innovatively provides an effective and safe strategy for neoadjuvant chemo-immunotherapy in TNBC.

2. Materials and methods

2.1. Ethics statement, mice, and cell lines

All human-related experimental procedures were reviewed and approved by the Clinical Ethics Committee of Changsha Yaxiang Biotechnology Co., Ltd. (AEWC-20220329-198). The tissue microassay is supported by AiFang Biological.

Female C57BL/6 and BALB/c mice of wild-type were sourced from Jiangsu Qinglongshan Biotechnology Co., Ltd. (Jiangsu, China). TLR2-deficient C57BL/6 mice were kindly provided by Prof. Lixin Wang. All animal studies were performed in compliance with the guidelines approved by the Institutional Animal Care and Use Committee of Nanjing University of Chinese Medicine (202409A043, AEWC-20220329-198).

The murine breast cancer cell lines (4T1, PY8119, and EO771) were procured from the Institute of Biochemistry and Cell Biology, Chinese Academy of Sciences (Shanghai, China) and the Chinese Tissue Culture Collection. Cells were cultured in Dulbecco's modified Eagle's medium (DMEM, VivaCell Biosciences, VivaCell Biosciences, C04001-500, Shanghai, China) or RPMI 1640, supplemented with 10% fetal bovine serum (FBS, VivaCell Biosciences, C04001-500, Shanghai, China), 100 U/mL penicillin, and 100 mg/mL streptomycin (Thermo Fisher Scientific, 15140-122 Waltham, MA, USA). All cell lines were maintained at 37 °C in a humidified atmosphere containing 5% CO_2.

2.2. Isolation and characterization of ADNPs

Fresh stems of *Astragalus membranaceus* were obtained from the *Astragalus membranaceus* Base (Datong, Shanxi, China) and rinsed twice with purified water at room temperature. The stems were ground using a slow juicer to extract the fresh fluid. The juice was then subjected to sequential centrifugation at 2000×*g* and 10,000×*g* to eliminate large debris and fibrous material. The resulting supernatant was ultracentrifuged at 100,000×*g* for 60 min (Beckman Coulter, Optima XE-100, Brea, CA, USA; Supporting Information Fig. S1). The pellet was resuspended in PBS, layered onto a sucrose gradient (8%, 15%, 30%, 45%, and 60%), and ultracentrifuged again at 100,000×*g*. After dilution in PBS, the sample underwent a final ultracentrifugation step at

100,000×*g* for 60 min. The final pellet was resuspended in sterile PBS and filtered through a 0.45 μm membrane for subsequent use.

2.3. The content of ononin and formononetin in different tissues was detected by the UPLC-Q-Orbitrap/MS method

Tissue separated from the liver, spleen, lung, and tumor of mice was quickly frozen in the −80 °C after PBS cleaning and precipitated with 1 mL methyl alcohol. Then, 100 mg of homogenized glass beads was added to grind and mix. Pooled quality control samples were prepared by mixing equal (2.00 mg/mL) amounts of each tissue sample. All samples were subsequently centrifuged at 13,000×*g* for 10 min at 4 °C, and then the supernatant from each sample was transferred to another 2 mL centrifuge tube. The supernatants were concentrated to dryness in a vacuum, following dilution with pure methanol successively. For ADNPs, the samples were diluted for analysis. The supernatants were subjected to metabolomics profiling by UPLC-Q-Orbitrap/MS after being filtered through a 0.22 μm membrane.

Chromatographic separation was used with an Agela Venusil C18 Plus 50 mm × 2.1 mm, 5 μm column maintained at 40 °C. The temperature of the autosampler was 8 °C. The mobile phase consisted of 0.1% formic acid in water (eluent A) and acetonitrile (eluent B) at a flow rate of 0.35 mL/min. Injection of 5 μL of each sample was done after equilibration. Gradient conditions were set as follows: 10% B isocratic 0.0 min, 10%−95% B linear 0.0−2.0 min, 95% B isocratic 2.0−3.8 min, 95%−10% B linear 3.8−4.0 min, and 10% B isocratic 4−5 min.

The ESI-MS experiments were used with the spray voltage of 4 kV in positive modes, respectively. Sheath gas and auxiliary gas were set at 50 and 15 arbitrary units, respectively. Respectively, the capillary temperature was 320 °C. The Orbitrap analyzer operated with a mass range of *m*/*z* 81−1000 for full-scan analysis at a resolution of 70,000. Data-dependent acquisition (DDA) MS/MS experiments were conducted using higher-energy collisional dissociation (HCD) scanning, with a normalized collision energy of 30 eV. Dynamic exclusion was applied to eliminate unnecessary information from the MS/MS spectra.

2.4. Cell viability assays

To better characterize the effect of ADNPs on cell proliferation. BMDMs, 4T1, and EO771 were treated by ADNPs for 48 h. Then, cell viability assays were performed by using the CCK8 kit (Yeasen, 40203ES80, Shanghai, China) following the indicated protocol.

2.5. DiO or DiI staining

ADNPs were stained with 5 μmol/L DiI (Invitrogen, V22885, Carlsbad, CA, USA)/DiO (Invitrogen, D275, Carlsbad, CA, USA) dye for 15 min at 37 °C. Then, ADNPs were centrifuged and washed with PBS with 10% serum 3 times. At last, the staining effect was evaluated by fluorescence detection.

2.6. Cellular uptake experiments

To better evaluate the ADNPs' biodistribution in various cells. 4T1, EO771, and BMDMs were treated with 10 μg/mL DiI-ADNPs for 12, 24, 36, or 48 h by flow cytometry assay to characterize the cellular uptake of ADNPs.

2.7. Macrophages and T lymphocytes co-culture experiments

To better assess the pharmacological action of ADNPs on $CD8^+$ T lymphocytes proliferation. $CD8^+$ T lymphocytes were extracted from the spleen of BALB/c mice with the CD8a microbeads kit (Miltenyi, 130-117-044, Bergisch Gladbach, Germany). We stained $CD8^+$ T lymphocytes with CFSE dye for 15 min and then co-cultured them with macrophages, which had been treated with or without ADNPs for 3 days. The proliferation of $CD8^+$ T lymphocytes was detected by flow cytometry.

2.8. Animal study design

To characterize the efficiency of ADNPs combined with Cisplatin by analyzing samples from mice with tumors. Three murine tumor models (EO711, 4T1-luc, and PY8119) were selected to evaluate the combinatorial treatment efficiency. 6-Week-old male mice were inoculated subcutaneously with 5×10^5 cells under the fourth breast pad ($n = 7-8$ per group, Day 0). The first treatment was scheduled until the tumor was around 50−100 mm^3 on Day 8. The Vehicle group received NS (100 μL/mouse/i.p.), Cisplatin (68 μg/100 μL/mouse/i.p., Beyotime, ST1164-10 mg, Shanghai, China), and ADNPs (200 μg/100 μL/mouse/i.p.) were injected intraperitoneally on Days 8, 11, 14, 17, and 20 as Fig. 2A demonstrates. The tumors were measured every other day with a caliper, and the volume was calculated according to Eq. (1):

$$\text{Tumor volume} = \text{Length} \times \text{Width}^2/2 \quad (1)$$

Mice with no visible or touchable tumors on consecutive days were considered to have completely regressed tumors. Mice were sacrificed when the tumor volume was over 2000 mm^3. Tumor weight was calculated by using an electronic weighing machine.

The 4T1 murine breast cancer lung metastasis study: 6-week-old female BALB/c mice were inoculated with 2×10^5 4T1 murine breast cancer cells in the right lower breast pad on Day 0. On Day 5, 1×10^5 4T1-luc murine breast cancer cells were intravenously injected to mimic the breast cancer lung metastasis. The treatment was started when the tumor volume in the breast pad was around 50−100 mm^3. Mice were sacrificed on Day 20, and their lungs were harvested and stored in Bouin's buffer (G-CLONE, RS 4140, Beijing, China).

To investigate tumor growth inhibition in the 4T1 murine TNBC model driven by ADNP-mediated TAMs polarization, 4T1-bearing BALB/c mice were treated with ADNPs in the presence of clodronate liposomes (CL, Yeasen, 40203ES80, Shanghai, China). Mice in the Vehicle group were treated with the same dose of liposomes containing PBS (PL, Yeasen, 40338ES10, Shanghai, China).

To analyze the role of TLR signaling pathways in macrophage polarization induced by ADNPs, TLR2-deficient C57BL/6 mice were implanted with PY8119 murine breast cancer cells.

The drug safety evaluation was performed by HE staining of main organs, the test of blood routine, liver and kidney function, EPO, MDA, and SOD analysis in whole blood or serum.

2.9. Colony-forming unit (CFU) assays

The methylcellulose-based medium with recombinant cytokines (including EPO) for mouse cells (STEMCELL, catalog#03434, Vancouver, Canada) was used. Bone marrow is extracted from 7-week-old C57BL/6 mice. 1×10^5 cells were treated with PBS,

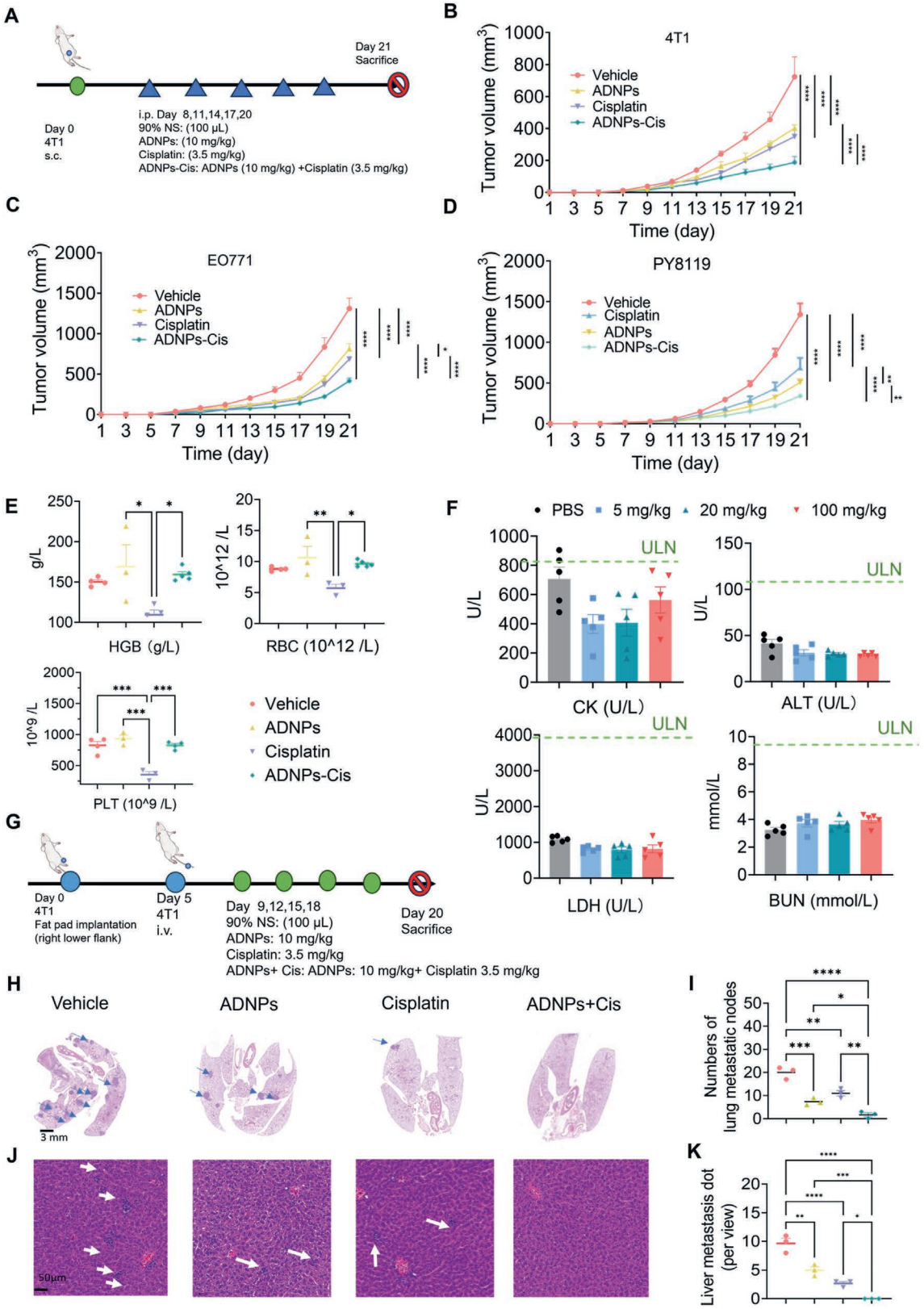

Figure 2 Combination therapy of ADNPs and Cisplatin (ADNPs-Cis) inhibits tumor growth in a 4T1 triple-negative breast cancer (TNBC) murine model. (A) Experimental schedule for tumor implantation and treatment administration. (B) Mean tumor volume in mice treated with Vehicle, ADNPs, Cisplatin, or ADNPs-Cis over time in the 4T1 murine model ($n = 5$ per group). (C) Mean tumor volume analysis of EO771 and (D) PY8119 in the TNBC tumor murine model. (E) Levels of hemoglobin (HGB), red blood cells (RBC), and platelets (PLT) *in vivo* ($n = 3$–5 per group). (F) Levels of creatine kinase (CK), alanine aminotransferase (ALT), lactate dehydrogenase (LDH), and blood urea nitrogen (BUN) *in vivo*.

Cisplatin, or ADNP + Cis for 7 days. The colony unit was calculated, and a representative image was taken at 4 × magnification of the microscope objective.

2.10. Tissue dissociation and flow cytometry

Tumor samples were minced with scissors before incubation with 0.5 mg/mL Collagenase IV (Yeasen, 40510ES60, Shanghai, China) and 0.1 mg/mL DNase (Yeasen, 10607ES15, Shanghai, China) in DMEM for 40 min at 37 °C. Single cell suspensions were prepared by filtering through 100 μm nylon filter strainers and washing. Immune cells were isolated from the tumor cell suspension using Percoll (GE Healthcare, 17-0891-09, Connecticut, CT, USA). Dead cells were excluded using Fixable Viability Dye (Invitrogen, 65-0866, Carlsbad, CA, USA), in combination with anti-CD16/32 monoclonal antibody (BioLegend, 101302, San Diego, CA, USA), by incubating for 15 min on ice in the dark. Then, cells were stained for 30 min in PBS with appropriate dilutions of various combinations of the following fluorochrome-conjugated antibodies, including anti-CD86 (b7-2) APC, anti-CD8a eFluor450, anti-NK1.1 APC, anti-Ly-6G Alexa Fluor647, anti-CD3 APC-eFluor 780, anti- CD16/32 purified, anti-CD25 super bright 436, anti-IL-6 APC, anti-CD19 APC, anti-CD4 APC, anti-CD11b APC/Cy7, anti-Ly-6C APC/Cy7, anti-CD69 FITC, anti-CD45 FITC, anti-CD11c Alexa Fluor 488, anti-F4/80 FITC, anti-CD62L Brilliant Violet 605, anti-CD103 PE, anti-CD206 PE, anti-CD11 b PE, anti-CD8a PE, anti-CD279 (PD-1) PerCP710, anti-F4/80 Brilliant Violet 421, anti-CD80 PE-Cy7, anti-CD45 PerCP/Cy5.5. For T cell-derived anti-tumor cytokines, 2×10^6 TILs were incubated in RPMI-1640 culture medium with Cell Stimulation Cocktail Plus Protein Transport Inhibitors (Invitrogen, 65-0866, Carlsbad, CA, USA) for 6 h. Then, the cells were stained with surface markers, fixed, and permeabilized using a Fixation/Permeabilization Kit (Invitrogen, 00-5521, Carlsbad, CA, USA) with anti-TNFα PE-Cy7, anti-FOXP3 PE, anti-Ki67 PerCP710, anti-IFN-γ Brilliant Violet 421, anti-Granzyme B PerCP/Cy5.5, and anti-CD45 PerCP/Cy5.5, which were diluted in the permeabilization buffer (Invitrogen, 00-8333, Carlsbad, CA, USA) and stained for 45 min. The flow cytometry assay is supported by Jiangsu Cell&Protein Biotechnology Co., Ltd.

2.11. Immunohistochemistry

Fresh organs such as the heart, liver, spleen, lung, and kidney were fixed. Hematoxylin and eosin staining was performed to analyze microscopic pathological changes in murine main organs under different treatments by an optical microscope (Olympus, Japan). Fresh tumor samples were fixed with 4% PFA for several days and embedded in paraffin, sectioned into 5-μm-thick sections, and observed using a Leica RM 2235154 (Leica, RM 2235154, Weztlar, Germany) after being mounted on adhesive glass slides. 5% BSA (Service Bio, 155 G50001, Wuhan, China) and CD8 (abcam, ab217344, Cambridge, UK) were used for staining to evaluate infiltration of CTLs in tumors. Ki67 (abcam, ab16667, Cambridge, UK) was used to evaluate the tumor cells' activity. The immunohistochemistry is supported by Wuhan Pinuofei Biological Technology Co., Ltd.

2.12. Confocal microscope and immunofluorescent

For immunofluorescence, BMDMs were fixed in 4% paraformaldehyde. Sections were washed three times with PBS for 5 min and mounted using DAPI (Beyotime, C1005, Shanghai, China) and imaged using 100 × magnification with a NIKON Eclipse ci with Case viewer software (3DHISTECH Ltd., 2.5 0.143918, Budapest, Hungary). The resultant digital images were analyzed using the NIS-Viewer. Image analysis was performed in Image J with the area measurement application or manual counting.

For DiI-ADNPs or formononetin-biotin-treated M2-BMDMs, sliced samples were fixed in ice-cold 4% paraformaldehyde. After being incubated with 5% BSA, they were incubated with TLR2-FITC/formononetin-biotin overnight at 4 °C and biotin-AF549 for another 2 h. The NICON Eclipse Ti (Nicon, Eclipse Ti, Tokyo, Japan) microscope was used to analyze the colocalization between TLR2 and ADNPs/Formononetin. The immunofluorescent confocal assay is supported by Wuhan Servicebio Technology Co., Ltd.

2.13. Preparation of protein samples and pull-down

The cell lysate (1 × cocktail protease inhibitor) was prepared at 4 °C, and the protein concentration was quantified using the BCA assay. A 50 μL cell sample and 250 μL of TBS were added into the PierceTM spin column (Pierce, 89879, Rockford, IL, USA) and centrifuged at $1000 \times g$ for 50 s to remove the TBS. Then, 300 μL of biotin (5 mmol/L) along with the formononetin-conjugated biotin was introduced to the spin column and incubated for 60 min, which was terminated by biotin blocking solution and rinsed with TBS. A total of 300 μL of protein trapping solution was used to capture formononetin-conjugated biotin, followed by washing with 250 μL of washing buffer. The protein was then resuspended in 2 × loading buffer, separated by electrophoresis, and the band of interest was excised for further analysis. The experimental process and data analysis were performed by TGTMED Co., Ltd. (Shanghai, China).

2.14. Identification by mass spectrometer

The samples underwent sequential washing steps using ultrapure water, de-staining solution, acetonitrile, and NH_4HCO_3. Following this, the proteins were subjected to reduction and alkylation using dithiothreitol (DTT) and iodoacetamide, respectively, and subsequently digested with trypsin. The resulting peptides were dried and then reconstituted in a buffer solution composed of acetonitrile, water, and formic acid. For desalination, the dried peptides were processed using a Ziptip C18 column (Merck KGaA, CB6574718, Darmstadt, Germany) and redissolved in 0.1% formic acid prior to analysis by mass spectrometry. The mass spectrometer was operated under the same parameter settings as previously described. Peptide identification and data analysis were performed using Proteome Discoverer 2.4 software (Thermo Fisher Scientific, Proteome Discoverer 2.4, Waltham, MA, USA).

(G) Experimental time schedule for the 4T1 TNBC lung metastasis murine model and treatment administration. (H) Representative HE images of lung metastases and (I) corresponding quantitative analysis ($n = 3$ per group; Scale bar = 3 mm). (J) Representative HE images of liver metastases and (K) corresponding quantitative analysis (Scale bar = 50 μm). *$P < 0.05$, **$P < 0.01$, ***$P < 0.001$, ****$P < 0.0001$. Data are presented as mean ± SEM and analyzed by two-way ANOVA or one-way ANOVA.

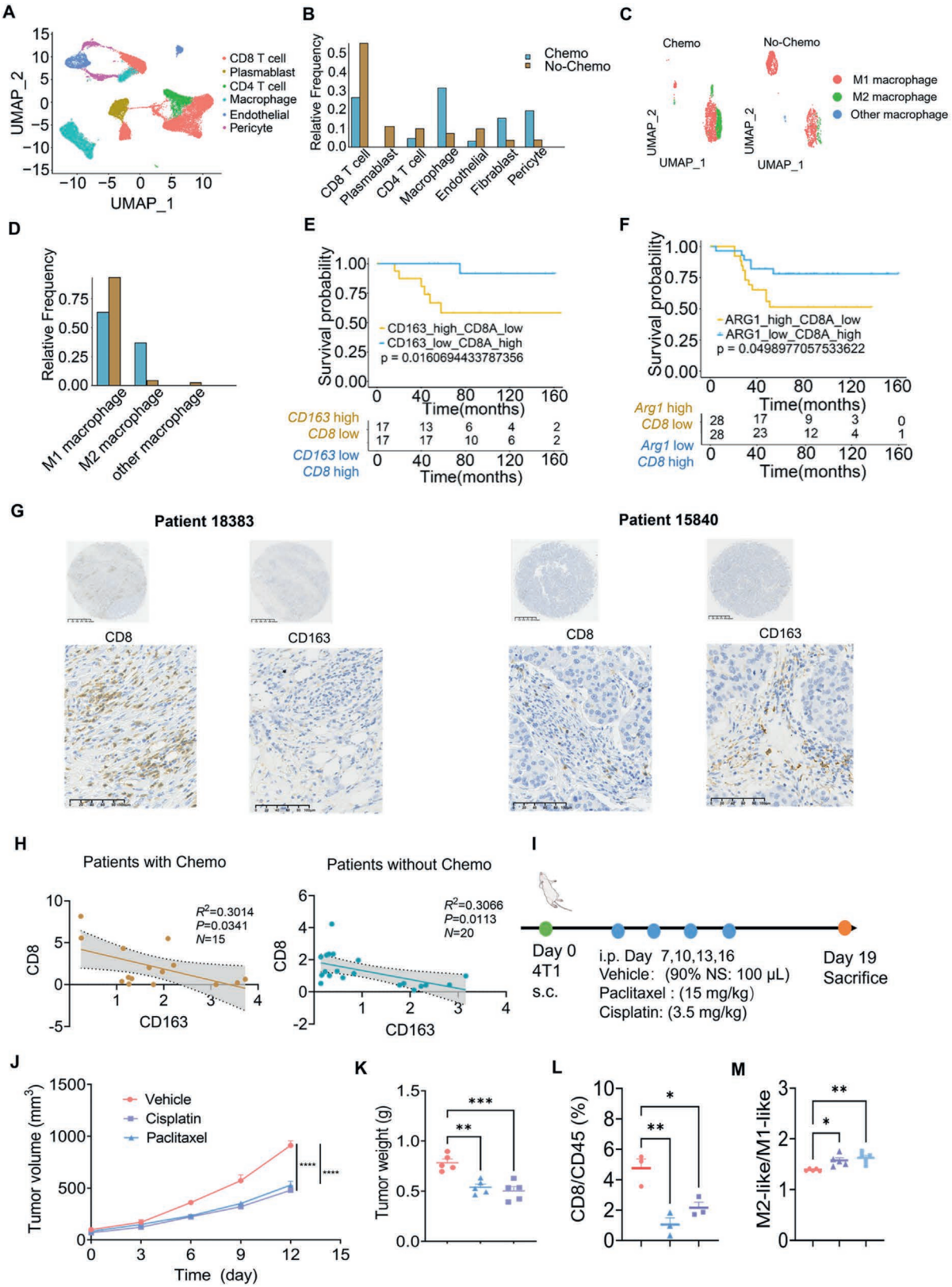

Figure 3 Single-cell RNA sequencing (scRNA-seq) analysis of the tumor microenvironment (TME) in TNBC patients. (A) UMAP visualization of major cell populations within TNBC tumors. (B) Comparative analysis of immune cell frequencies in the TME of TNBC patients with and without chemotherapy. (C) UMAP visualization of macrophages within TNBC tumors. (D) Changes in macrophage subtype frequencies in the TME of TNBC patients with and without chemotherapy. (E) Kaplan−Meier survival analysis of TNBC patients from the TCGA database stratified by $CD163^{high}CD8A^{low}$ and $CD163^{low}CD8A^{high}$ expression ($P = 0.016$). (F) Kaplan−Meier survival analysis of TNBC patients from the

The experimental process and data analysis were performed by TGTMED Co., Ltd. (Shanghai, China).

2.15. Molecular docking

The ligand structure of TLR2, initially in Mol2 format, was transformed into PDB format using Chem3D software (PerkinElmer Informatics, V14.0.0.117, Waltham, MA, USA). Subsequently, the three-dimensional (3D) structures of SQLE and HMGCR in PDB format were retrieved from the Protein Data Bank (PDB). These structures were then processed to remove water molecules and add hydrogen atoms using PyMOL software (http://www.PyMOL.org). For molecular docking analysis, AutoDock Tools 1.5.6 was employed to identify the active binding pockets, define the grid box coordinates and dimensions, and assess the interaction between the core ligand and target proteins. The docking results were visualized and analyzed using PyMOL.

2.16. Molecular dynamics simulation

The molecular dynamics simulation of the ligand bound to TLR2 (PDBID: 6NIG) complexes was conducted by GROMACS 2022. Firstly, the initial conformation of the ligand was generated by AutoDock Vina (1.2.0). The parameter files of the ligand were obtained from SwissParam (www.swissparam.ch). The model system was filled with dodecahedron TIP3 water, and Na^+/Cl^- was added to ensure electrical neutrality. MD simulations of the model systems were completed for 100 ns at a constant temperature of 310 K. Trajectories of simulations were further analyzed and visualized by UCSF ChimeraX (version: 1.9rc202411270810) and Discovery Studio Visualizer (BIOVIA Discovery Studio 2019, Dassault Systèmes, San Diego, CA, USA), while the Root Mean Square Deviation (RMSD) was calculated using GROMACS 2022.

2.17. Bioinformatic analyses

Computational analyses were conducted using the R software environment for statistical computing and graphical visualization. For triple-negative breast cancer (TNBC) tumors, single-cell mRNA expression data were obtained from the Expression Project for TNBC (expO; http://www.intgen.org/) and analyzed using publicly available datasets (GEO accession numbers: GSE176078 and GSE58812).

2.18. Statistical analyses

Data are presented as mean ± standard error of the mean (SEM). Statistical evaluations were performed using GraphPad (GraphPad Software, Prism 9.5.0, San Diego, CA, USA). Depending on the experimental design, appropriate statistical tests were applied, including unpaired Student's *t*-test, one-way or two-way analysis of variance (ANOVA), and the log-rank (Mantel−Cox) test. A *P*-value of less than 0.05 was considered statistically significant, with significance levels denoted as follows: $*P < 0.05$, $**P < 0.01$, $***P < 0.001$, and $****P < 0.0001$.

3. Results

3.1. Elevated M2-like macrophages and reduced $CD8^+$ T cells in post-chemotherapy tumors in TNBC patients with poor prognosis

Firstly, we evaluated the immune cell subtypes in the TME of TNBC patients using publicly available datasets of scRNA sequencing. A diverse range of cell types within the TME including macrophage, $CD4^+$ T lymphocytes, $CD8^+$ T lymphocytes, plasma blast, endothelial, and pericyte were analyzed (Fig. 3A). Macrophages and $CD8^+$ T lymphocytes were the most abundant immune cell subtypes in TNBC patients with chemotherapy (Fig. 3B). Next, investigation of the chemotherapy effects on the immune cell composition within the TME. Compared to chemotherapy-naive (untreated) tumors, post-chemotherapy triple-negative breast cancer (TNBC) tumors showed a marked reduction in cytotoxic immune cells—such as $CD8^+$ T lymphocytes, $CD4^+$ T lymphocytes, and plasmablasts—as well as a decline in endothelial cells. Conversely, these tumors exhibited an increase in M2-like tumor-associated macrophages (TAMs, Fig. 3C and D), fibroblasts, and pericytes (Fig. 3B). However, analysis of the TCGA data set suggests an association of higher levels of M2-like TAMs ($CD163^{High}$ or $ARG1^{High}$) and the lower levels of $CD8^+$ T lymphocytes with worse survival outcomes (Fig. 3D−F). Additionally, immunohistochemistry analysis of tumor tissues from TNBC patients confirmed the abundance of $CD8^+$ T cells and M2-like TAMs are inversely correlated (Fig. 3G). Our data showed a negative correlation between the CD163 and CD8 expression in TNBC tumor samples, both in patients with chemotherapy and patients without chemotherapy, indicating that higher M2-like TAMs were accompanied by lower $CD8^+$ T cells in all TNBC patients (Fig. 3H).

As the application of paclitaxel and platinum are commonly used in TNBC clinical treatment, we compared the treatment efficiency of paclitaxel and platinum and analyzed the TME in 4T1 breast cancer murine model (Fig. 3I). The results showed that both paclitaxel and Cisplatin could efficiently inhibit 4T1 breast cancer tumour volume and tumour weight (Fig. 3J and K, Supporting Information Fig. S2A). Neither chemotherapies altered the mice's body weight (Fig. S2B). In comparison to the Vehicle group, the paclitaxel and Cisplatin group exhibited a rise in M2-like/M1-like macrophages and a decline in $CD8^+$ T/$CD45^+$ cells (Fig. 3L and M), aligning with the scRNA-seq results from TNBC tissues. These results imply that enhancing $CD8^+$ T lymphocyte levels while reducing M2-like TAM generation in the post-chemotherapy tumour microenvironment may lead to better survival outcomes for TNBC patients.

3.2. The biophysical characterization of astragalus-derived exosome-like nanoparticles (ADNPs)

Astragalus has been reported to have the ability to effectively improve the TME and enhance tumour therapy[27]. Plant-derived nanoparticles have shown better pharmacological characteristics

TCGA database stratified by $ARG1^{high}CD8A^{low}$ and $ARG1^{low}CD8A^{high}$ expression ($P = 0.049$). (G) Representative immunohistochemical (IHC) staining of CD8 and CD163 in tumor tissue microarrays from TNBC patients. Scale bar = 100 μm. (H) Correlation analysis of CD8 and CD163 expression in chemotherapy-treated *versus* untreated TNBC patients (Patient 18,383: untreated; Patient 15,840: treated). (I) Two major clinical chemotherapies in the 4T1 murine triple negative breast cancer model time schedule. (J) Tumor volume analysis (K), Tumor weight (L), CD8/CD45, and (M) M1/M2 in TME. Data are presented as mean ± SEM. $*P < 0.05$, $**P < 0.01$, $***P < 0.001$, $****P < 0.0001$.

in immune regulation[31]. However, it is unknown whether astragalus-derived ADNPs possess anti-tumour bioactivity in TNBC. To investigate this, we first isolated ADNPs from fresh Astragalus through a series of processes including juicing, filtration, and differential centrifugation (Supporting Information Fig. S1). ADNPs exhibited a size distribution between 200 and 300 nm by nanoparticle tracking analysis (NTA) (Fig. 4A). Besides, ADNPs were characterised as bi-layered and oval-shaped nanovesicles in transmission electron microscopy (TEM) (Fig. 4A). The ADNPs exhibited a mean surface potential of −24.741 mV measured by dynamic light scattering (DLS) (Supporting Information Fig. S3A). Initially, the pellets were resuspended in PBS and subsequently layered onto a sucrose gradient solution comprising concentrations of 8%, 15%, 30%, 45%, and 60%. Following ultracentrifugation at 100,000×*g* for 1 h, the vesicle fraction, predominantly concentrated in the 15% sucrose layer, was carefully harvested for further analysis (Fig. 4B). Additionally, we showed that ADNPs have a high temperature stability and pH stability, evidenced by retained structural integrity and grain size at temperatures of 80 and −80 °C, as well as in simulated gastric and intestinal fluids (Fig. S3B). Furthermore, the physical structure of ADNPs was degraded when exposed to DNase and protease (Fig. S3B), indicating instability of ADNPs in an enzymatic environment. By using a high-throughput non-targeted lipidomic and metabolomic analysis, we showed that ADNPs comprise the vast majority of sphingomyelin (∼80%) and ceramide (∼4%), similar to common cellular components (Fig. S3C). ADNPs contained two representative bioactive components of Astragalus, the formononetin and ononin, while notably lacking the astragaloside (Fig. S3D). While the measured protein concentration varied between batches due to differences in dilution volumes or harvest seasons, no significant differences were observed in the mean concentrations of active compounds (*e.g.*, formononetin) when batches were normalized to the same protein concentration (Fig. S3D). Thus, we speculated that ADNPs may include small molecules, lipids, DNA, and proteins inside (Fig. S3E). To better evaluate the biofunction of ADNPs, the DiI-stained ADNPs were characterized. The DLS measurements, zeta potential, and relative fluorescent intensity of DiI-ADNPs demonstrated excellent stability over several days, ensuring reliable performance for both *in vivo* and *in vitro* experiments (Fig. S3F).

Next, to explore whether ADNPs affect tumour cell activity *in vitro*, we analysed the cell viability after different concentrations of ADNPs in multiple breast cancer cell culture systems. Our data showed that ADNPs failed to inhibit the activity of 4T1 and EO771 cells (Supporting Information Fig. S4A). This is likely due to the minimal levels of ADNPs uptake by tumour cells. In 4T1 cells, ADNPs were taken up by less than 1% of tumour cells after 48 h of ADNPs treatment (Fig. 4C). In EO771 cells, the uptake efficiency of ADNPs was 1.06% in 48 h, approximately double that of 24 h, indicating that prolonging the treatment period did not improve the efficacy of ADNPs uptake in tumour cells (Fig. 4C).

To further explore the direct effects of ADNPs on other immune cells, we examined the phagocytosis of ADNPs within the splenocytes *in vivo*. The proportion of macrophages phagocytosing ADNPs was significantly higher than that of other immune cells (Fig. 4D). Following 36 h of exposure to ADNPs, approximately 27.5% of bone marrow-derived macrophages (BMDMs) exhibited uptake of the nanoparticles, and the phagocytic activity demonstrated a progressive increase over time (Fig. 4E), suggesting that ADNPs showed a great tropism for macrophages compared with other immune cells and tumor cells. Next, the localization of DiI-labeled ADNPs in macrophages also indicates the targeting ability of ADNPs in macrophages (Fig. 4F). Besides, our data suggested that the phagocytosis of ADNPs was significantly inhibited after treatment with macropinocytosis inhibitor EIPA, whereas treatment with the phagocytosis inhibitors Filipin III and Nocodazole had no significant effect (Fig. S4B), indicating that macrophages may predominantly uptake ADNPs through a macropinocytosis-mediated pathway.

To investigate the biodistribution of ADNPs *in vivo*, mice administered with DiO-ADNPs by i.p. were sacrificed after 72 h. We confirmed that ADNPs were stably present in the spleen, liver, lungs, and tumour tissues of mice (Fig. S4C). Two bioactive components of Astragalus in ADNPs, *i.e.*, formononetin and ononin, were detected predominantly in the lung, liver, and spleen, respectively (Fig. S4D). Additionally, formononetin and ononin were both detected in the liver, spleen, and lungs (Fig. S4D), which indicated that ADNPs may target the organs prone to TNBC metastasis. To assess the protein composition of ADNPs, we analyzed their protein expression profiles both before and after enzymatic treatment with DNase I or proteinase K. The results revealed a marked decrease in protein expression following proteinase K digestion, confirming the presence of protein components within the ADNPs (Fig. S4E).

3.3. ADNPs combined with Cisplatin (ADNPs-Cis) therapy effectively inhibit TNBC progression and reduce the toxic side effects of Cisplatin

While the paclitaxel and platinum are both first-class clinically applicable drugs for TNBC, the platinum showed a better 5-year DFS and lower tumour recurrence in TNBC[32,33]. This led us to establish a combination of ADNPs and Cisplatin (ADNPs-Cis) treatment for TNBC. To assess the effect of ADNPs-Cis in TNBC, we established a tumour-bearing murine model by orthotopically implanting 4T1 breast cancer murine cells into the right fourth mammary pad of BALB/c mice for 21 days. Mice were divided into four groups treated with (a) 90% saline, (b) ADNPs, (c) cisplatin, or (d) ADNPs-Cis every three days from Day 8 to Day 20 (Fig. 2A). No significant change in body weight was found among different groups (Supporting Information Fig. S5A). The tumour volume analysis and representative tumour image showed that 4T1 tumour growth was significantly inhibited in all treatment groups (Figs. 2B, S5B). Though the treatment of ADNPs alone showed a less inhibitory effect on tumour volume than treatment of Cisplatin alone, ADNPs-Cis treatment further strengthened the inhibitory effects on tumour volume compared to treatment of Cisplatin alone (Fig. 2B). Consistently, the tumour mass was conspicuously reduced in ADNPs-Cis compared with the cisplatin or ADNPs treatment alone (Fig. S5C). The improved inhibitory effects of ADNPs-Cis on tumour growth were observed in other murine TNBC models (EO117 and PY8119) (Fig. 2C and D, Supporting Information Figs. S5D−S5G, S6A−S6D). Notably, mice treated with ADNPs-Cis showed improved survival time compared to those in other groups, indicating that the ADNPs-Cis significantly inhibits TNBC tumour progression with maintained safety in mice (Fig. S6E).

Furthermore, histological analysis revealed that the ADNPs-Cis-treated mice exhibited significantly fewer mitotic cells in tumour cells compared to the Cisplatin group, suggesting an

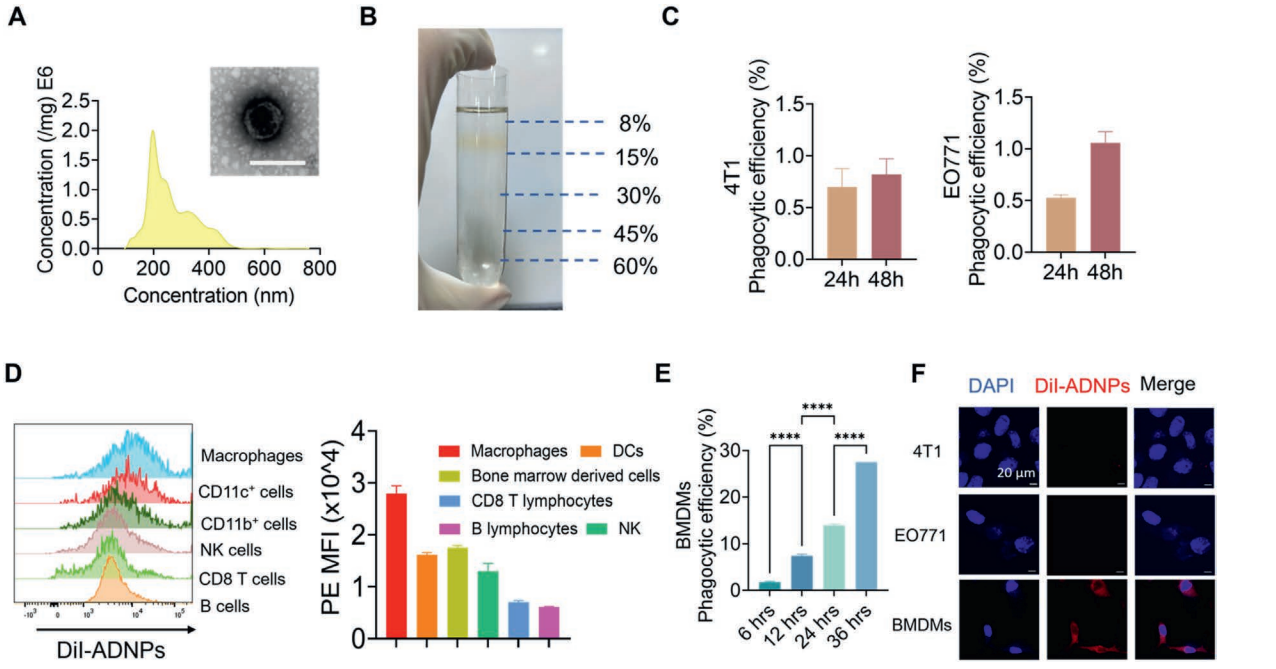

Figure 4 Characterization of ADNPs isolated from fresh *Astragalus membranaceus*. (A) Nanoparticle tracking analysis (NTA) and transmission electron microscopy (TEM) image of ADNPs (scale bar = 200 nm). (B) Purification of fresh *Astragalus membranaceus* juice using sucrose density gradient centrifugation. (C) Phagocytic efficiency of ADNPs by 4T1 and EO771 cells. (D) Quantitative flow cytometry analysis of DiI-labeled ADNPs uptake by various immune cell subsets (n = 3−5 per group). (E) Time-dependent phagocytic efficiency of ADNPs by bone marrow-derived macrophages (BMDMs) (n = 2−3 per group, ***$P < 0.0001$). (F) Confocal microscopy images showing uptake of DiI-labeled ADNPs (2 μg/mL) by 4T1, E0771, and BMDMs after 12 h of incubation (scale bar = 20 μm). Data are presented as mean ± SEM.

inhibition of tumour cell proliferation (Fig. S6F). Protein expression of Ki67 was also significantly reduced in the ADNPs group, Cisplatin group, and ADNPs-Cis group compared to the Vehicle group, indicating a reduced proliferation ability of tumor cells in the treatment groups (Fig. S6G).

To further assess the safety of the ADNPs-Cis *in vivo* treatment, the blood from mice in 4 groups was collected and analysed. Our experimental results revealed that compared with the Cisplatin treatment group, ADNPs and ADNPs-Cis therapy reversed the reduction of red blood cell counts, platelets, and haemoglobin in Cisplatin-treated mice (Fig. 2E). In addition, CK, ALT, LDH, and BUN were in safe ranges under different concentrations of ADNPs, indicating the minimal cardiotoxicity and nephrotoxicity of ADNPs at different concentrations (Fig. 2F). No significant difference was found in kidney function and blood routine *in vivo* (Supporting Information Fig. S7A−S7F). To better clarify the function of ADNPs in hematological toxicity improvement. The MDA, SOD and EPO were detected in murine serum. In line with the fact that Cisplatin was reported to reduce EPO and SOD level, however, ADNPs were found to restore the functions of EPO (Fig. S7G) and SOD (Fig. S7H), despite that SOD level was slightly lower than that of the control group. Meanwhile, Cisplatin significantly increases the MDA level, which was largely reduced by the ADNPs treatment (Fig. S7I). Besides, to better evaluate the anti-myelosuppression of ADNPs, the colony-forming assays were performed, and the results showed that the ADNPs could efficiently protect the cloning ability of bone marrow stem cells compared with that destroyed by Cisplatin (Fig. S7J). Additionally, the analysis of hematoxylin-eosin (HE) staining in multiple organs revealed no significant pathological change among treatment groups (Supporting Information Fig. S8A). Together, our study suggests that ADNPs-Cis therapy effectively inhibits the TNBC progression and reduces the toxic side effects of Cisplatin.

Given that the mortality and eligibility of surgery are associated with tumour metastasis, we evaluated ADNPs-Cis therapy on TNBC metastasis using the 4T1 breast cancer lung metastasis murine model (Fig. 2G). To better characterize the combinatorial treatment efficiency in decreasing lung metastasis, HE staining was performed (Fig. 2H), and the results showed that ADNPs-Cis significantly reduced 90% of lung metastatic foci in the lung compared to ADNPs or Cisplatin group (Fig. 2I). Furthermore, we also observed elimination of liver metastatic foci by HE staining (Fig. 2J) *in situ* spontaneous transfer mode; the results showed that ADNPs-Cis treatment is better than ADNPs or Cisplatin treatment in liver metastasis suppression (Fig. 2K). Together, our data suggest that ADNPs-Cis therapy effectively inhibits tumour metastasis.

3.4. ADNPs-Cis therapy effectively reprograms TAMs to enhance the beneficial effects of Cisplatin on the TME

To gain deeper insights into the impact of ADNPs-Cis on the tumor microenvironment (TME) in triple-negative breast cancer (TNBC), we conducted a comprehensive analysis in subpopulations of TAMs and T lymphocytes in the TME. Flow cytometry analysis indicated a significantly greater immune cell infiltration in three treatment groups compared to Vehicle group, with markedly higher infiltration of immune cells (CD45/live cells) in the ADNPs-Cis group than either the ADNPs or Cisplatin groups alone (Fig. 5A). The proportion of macrophages were comparable among four groups (Fig. 5B). Treatment with ADNPs

alone or in combination with Cisplatin resulted in a markedly increase in M1-like TAMs, a decline in M2-like TAMs compared to Cisplatin and Vehicle groups (Fig. 5C and D), and an elevated ratio of M1/M2 TAMs in tumor tissues compared to the Cisplatin and Vehicle groups (Fig. 5E), indicating that ADNPs promote the increase of M1-TAMs and the reduction of M2-TAMs in 4T1 TNBC murine models.

Next, to investigate whether ADNPs exert their anti-tumour effects through macrophages, we injected clodronate liposome (CL) into TNBC tumour mice to eliminate macrophages. Firstly, we confirmed that the macrophages were effectively eliminated after CL treatment (Supporting Information Fig. S9A and S9B). The following research indicates that ADNPs-Cis treatment in macrophage-lacking mice failed to trigger the inhibitory effects on tumour growth, suggesting that depletion of macrophages neutralizes the effects of ADNPs-Cis on tumour suppression (Fig. S9C−S9F). These findings indicated that ADNPs inhibit tumour growth through a TAM-dependent mechanism.

3.5. ADNPs activate tumor-infiltrating T lymphocytes in the TME

Macrophages are recognized as important antigen-presenting cells in TME, which not only activate T lymphocytes but also directly improve anti-tumor immune activity[14]. T lymphocytes are one type of immune cell that directly kill tumor cells in the TME. Next, we investigated the effects of ADNPs-Cis treatment on the tumor-infiltrating T cells. The findings revealed that administration of ADNPs-Cis led to a notable enhancement in the infiltration of $CD3^+$ T lymphocytes relative to both the Vehicle and Cisplatin treatment groups (Fig. 5F). Furthermore, our data showed a significant elevation of the $CD8^+$ T lymphocytes proportion in the

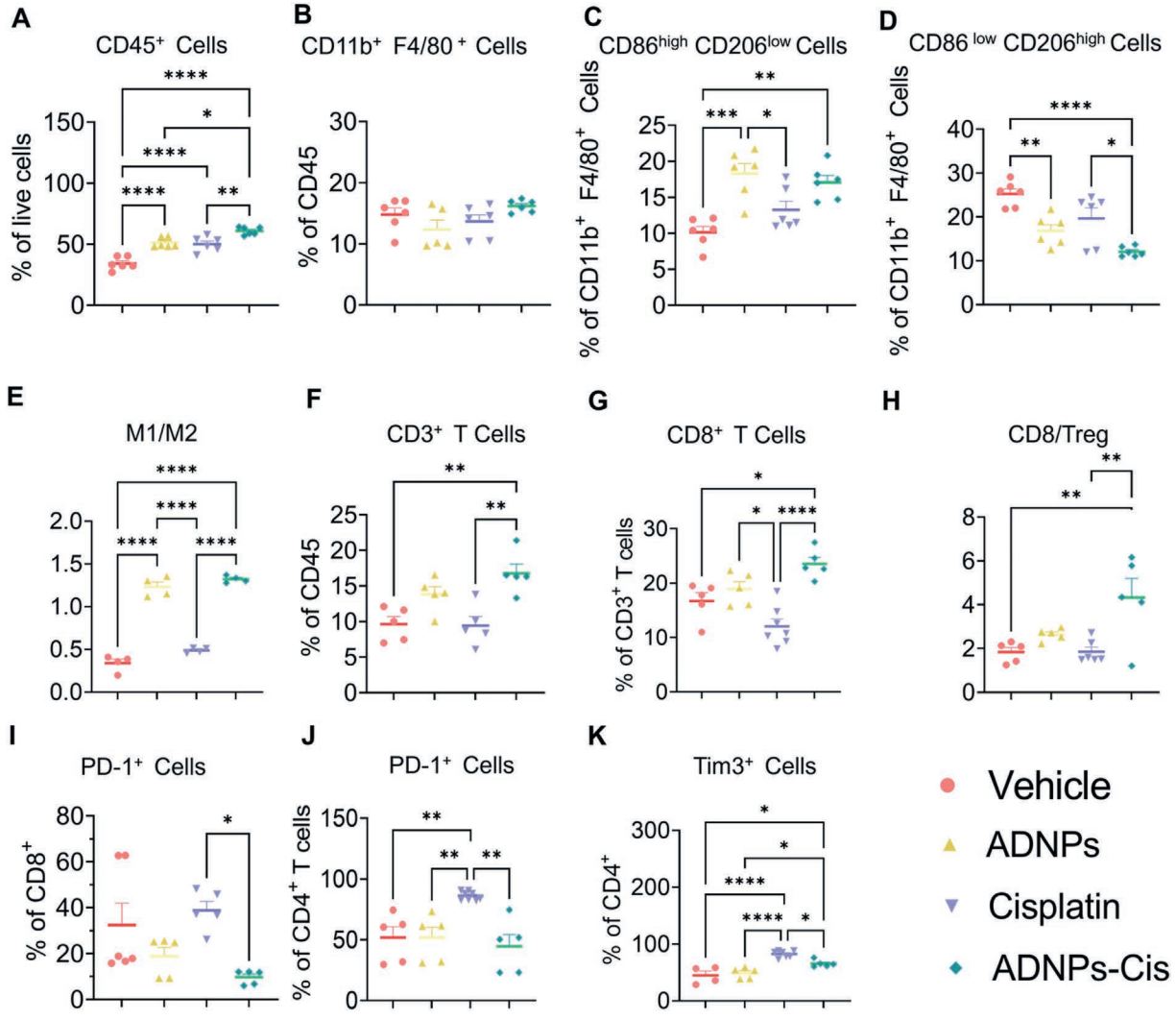

Figure 5 Analysis of T lymphocyte phenotypes and macrophage subtypes in TME. (A) Proportion of CD45 cells in live cells ($n = 6$ per group). (B) Ratio of macrophages to $CD45^+$ T cells ($n = 5-6$ per group). (C) Proportion of $CD86^{high}CD206^{low}$ macrophages in TAMs ($n = 6$ per group). (D) Proportion of $CD86^{low}CD206^{high}$ macrophages among TAMs ($n = 6$ per group). (E) Ratio of M1-like to M2-like macrophages ($n = 4$ per group). (F) Proportion of CD3 lymphocytes in CD45 cells ($n = 5$ per group). (G) Ratio of $CD8^+/CD3^+$ T lymphocytes ($n = 5-7$ per group). (H) Ratio of $CD8^+$ to Treg ($n = 5-6$ per group). (I) Flow cytometry analysis of PD-1^+ $CD8^+$ T, (J) PD-1^+ $CD4^+$T cells, and (K) $TIM3^+CD4^+$T in the tumor ($n = 4-7$ per group). $^*P < 0.05$, $^{**}P < 0.01$, $^{***}P < 0.001$, $^{****}P < 0.0001$. Data are presented as mean ± SEM and analyzed by one-way ANOVA.

ADNPs and ADNPs-Cis treatment groups compared with the cisplatin group (Fig. 5G). As tumor immune escape by promoting the expansion of Treg in TME can suppress the activation of $CD8^+$ lymphocytes. Our data demonstrated that the ratio of $CD8^+$/Treg cells was dramatically elevated in the ADNPs-Cis group compared to the Cisplatin and Vehicle groups (Fig. 5H), confirming the efficacy of ADNPs-Cis treatment in reversing the immunosuppressive environment. The exhausted T lymphocytes were also been detected, ADNPs-Cis treatment significantly reduced the expression of PD-1 on the surface of $CD8^+$ T lymphocytes (Fig. 5I), and downregulated TIM3 and PD-1 expression of $CD4^+$ T lymphocytes compared with Cisplatin treatment only (Fig. 5J and K), which indicated the alleviating of T lymphocytes exhaustion in TME caused by cisplatin application.

In the following research, we analysed the cytotoxic function of $CD8^+$ T cells within the tumours. ADNPs markedly increased the levels of IFN-γ, Granzyme B, and TNF-α in the $CD8^+$ T cells compared with the Vehicle or Cisplatin group (Fig. 6A−C). However, the combinatorial treatment did not show an obvious benefit compared with single treatment. Additionally, ADNPs enhanced $CD8^+$ T lymphocyte proliferation, as evidenced by a 16% increase in Ki67-expressing $CD8^+$ T lymphocytes compared to the Cisplatin group (Fig. 6D). Besides, the HE staining showed ADNPs-Cis treatment significantly enhanced the infiltration of $CD8^+$ T lymphocytes into the tumour compared to the Vehicle group (Fig. 6E). ADNPs-Cis and ADNPs treatment resulted in an elevated proportion of $CD4^+$/IFN-γ^+ (Fig. 6F), $CD4^+$/Granzyme B^+ (Fig. 6G), and $CD4^+$/TNF-α^+ (Fig. 6H) cells compared to the Cisplatin group. As an improvement of tumour-related immune memory cells, indicating the activation of the anti-tumour immune system, we assessed the effects of ADNPs-Cis on tumour memory in splenocytes 63 days after tumour decollement. Our data showed that mice treated with ADNPs-Cis or ADNPs showed higher proportions of central memory T lymphocytes and effective memory T lymphocytes in both $CD4^+$ and $CD8^+$ T lymphocytes compared with the Cisplatin group (Supporting Information Fig. S10A), suggesting that ADNPs-Cis treatment could trigger a durable anti-tumour immune memory.

M2 macrophages play the invariable role in modulating $CD8^+$ T lymphocytes proliferation and activation by creating an immunosuppressive TME[34]. To investigate whether ADNPs-modulated anti-tumour effects of $CD8^+$ T cells were M2 macrophage-dependent, we constructed a co-culture system of M2-BMDMs and CD3/CD28-stimulated $CD8^+$ T cells (Fig. 6I). To assess the immunosuppressive effects of M2 macrophages, we tested the effects of ADNPs treatment on $CD8^+$ T lymphocytes proliferation. A markedly increased proliferation rate of $CD8^+$ T lymphocytes was detected in the group treated with ADNPs when compared to the non-ADNP-treated group (Fig. 6J and K).

To better clarify the macrophage immune function regulated by ADNPs, we performed a series of *in vitro* assays. Our data showed that mRNA levels of *Il-6*, *Tnfα*, *Cxcl9*, *Inos*, *Tlr2*, and *Cd86* were significantly upregulated in ADNPs-treated BMDMs (Fig. 7A). However, they reached a peak at 6 h and reduced mRNA levels later, which is likely due to the transcriptional repression of inflammation-associated genes.

Besides, the ADNPs treatment also significantly promoted ROS production in M2-BMDMs (Fig. 7B). And the protein expression of CD206, the characteristic surface marker of M2 macrophages, was significantly lower in the M0 and M2+ADNPs groups compared to the M2 group. We further assessed the protein levels of CD80 and CD86, characteristic markers of M1 macrophages, while there was no significant difference in CD80 and CD86 expression between the M0 and M2 group, ADNPs treatment of the M2 group led to significantly higher CD80 and CD86 expression compared to the M2 group (Fig. 7C). Additionally, ADNPs enhanced the production of pro-inflammatory cytokines linked to the M1 phenotype, such as TNF-α, IL-8, and IL-6, while suppressing the expression of the M2-associated cytokine IL-10 (Fig. 7D). These findings demonstrate that ADNPs effectively drive the shift from an M2-like to an M1-like BMDMs.

3.6. Formononetin is the active compound of ADNPs to repolarize M1-like macrophages by the TLR2 signalling pathway

To investigate the mechanisms driving ADNPs-mediated polarization of M2-like macrophages, RNA-seq analysis was conducted on M2-BMDMs exposed to ADNPs. KEGG pathway enrichment analysis revealed a significant activation of the TLR signalling pathway in the ADNPs-treated group (Fig. 8A). The volcano plot analysis and differential gene analysis of TLR-related gene expression revealed a significant upregulation of TLR2 in ADNPs-treated M2-BMDMs (Fig. 8B and C). Consistently, the results also indicated the significant increases in the expression of proteins involved in the TLR2 pathway, including *p*-IKKβ, p-P65, p-P50, IκBα, and TLR2 in ADNPs-treated M2-like BMDMs (Fig. 8D and Fig. S10B). Then, we found co-localization of DiI-ADNPs with TLR2 in immunofluorescence with around 0.87 Pearson's *r* in TLR2 and DiI-ADNPs fluorescent space counting (Fig. 8E). Together, our data confirmed that ADNPs bind to TLR2 and activate downstream of the TLR2 signalling pathway in M2-BMDMs.

To further verify whether the immunomodulatory effect of ADNPs is regulated through the TLR2 pathway, we performed a pharmacodynamic study *in vivo* by using the py8119 murine breast cancer model in TLR2 knockout ($TLR2^{-/-}$) mice (Supporting Information Fig. S11A). The tumor restriction of ADNPs in the PY8119 murine model showed a better effect in WT mice than in $TLR2^{-/-}$. Besides, the $TLR2^{-/-}$ + ADNPs group significantly reduced tumor weight compared to that of the $TLR2^{-/-}$ group (Fig. S11B−S11D). ADNPs had a minimal effect on murine body weight in $TLR2^{-/-}$ mice (Fig. S11E). Although ADNPs decreased the tumour volume in $TLR2^{-/-}$ mice, it was less bulky in WT mice. Besides, the volume of spleen in $TLR2^{-/-}$ mice showed a larger size compared to the WT mice, although both groups exhibited a significant reduction in spleen size following ADNPs treatment (Fig. S11F). And the immunofluorescent analysis indicated that ADNPs were phagocytosed by BMDMs through TLR2 (Fig. S11G).

As the non-targeted mass spectrum analysis showed, ADNPs contain key pharmacologically active components, including formononetin and ononin. Then, we elucidated the polarization capacity of both active compounds on M2-BMDMs. The results showed that formononetin, but not ononin, effectively promoted the polarization of M1-BMDMs (Fig. 8F, Supporting Information Fig. S12A and S12B). These results demonstrate that formononetin could be the active compound in activating M2-like BMDMs in ADNPs, as formononetin has been found to have great ability in tumour reduction in previous research[35]. We performed an animal assay with three different treatments: (a) the same concentration of formononetin in ADNPs (F-low), (b) ADNPs, or (c) a concentration of formononetin in other murine tumour research (F-high) (Supporting Information Fig. S13A).

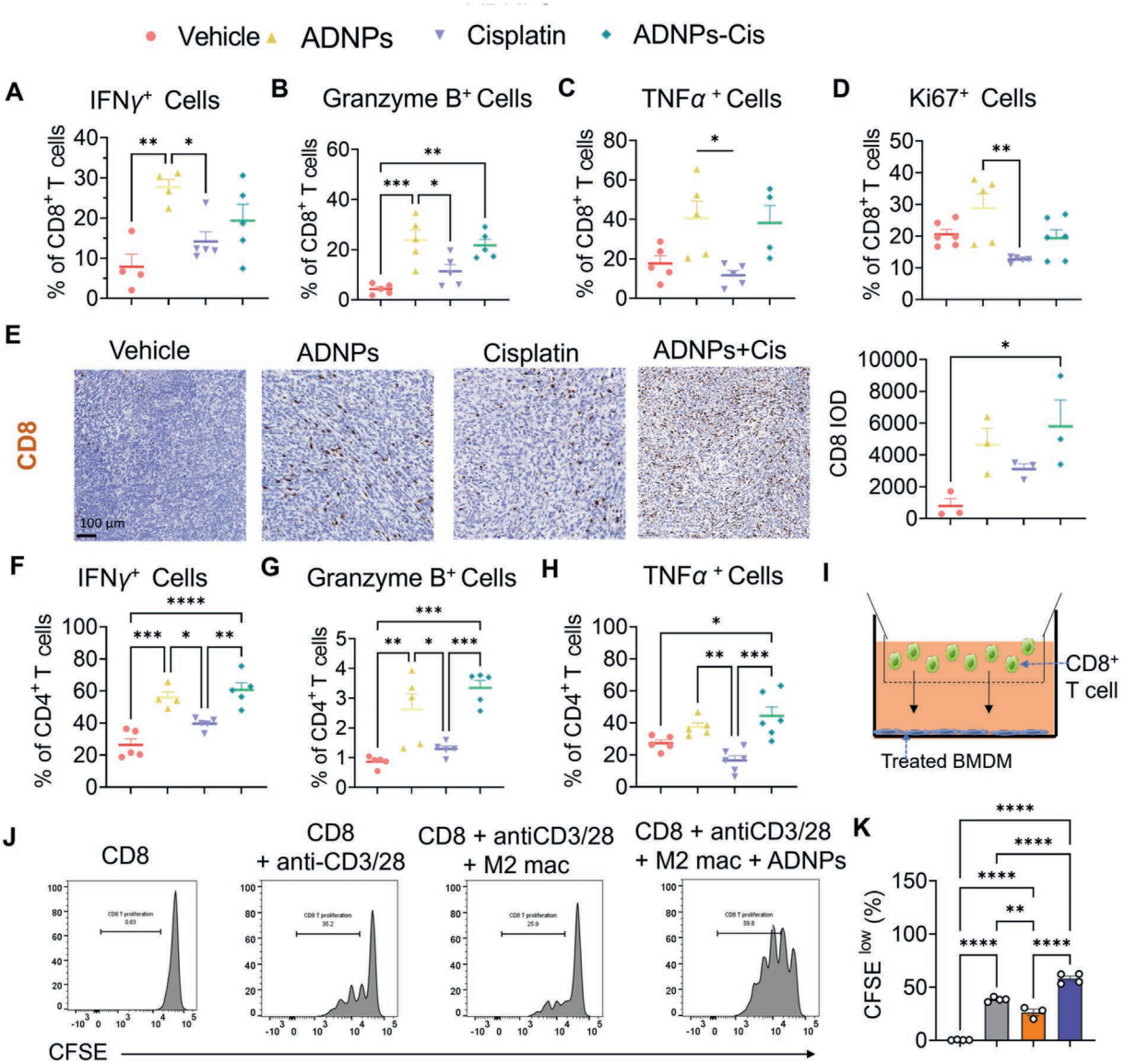

Figure 6 Analysis of T lymphocyte-related cytotoxic functions in the TME of 4T1 triple-negative breast cancer (TNBC) bearing mice treated with Vehicle, ADNPs, Cisplatin, or ADNPs-Cis. Proportion of (A) IFN-γ^+CD8$^+$, (B) Granzyme B$^+$CD8$^+$, (C) TNF-α^+CD8$^+$ (n = 4−5 for each group). (D) Ki67$^+$CD8$^+$ (n = 5−6 for each group) in CD8$^+$ T Cells. (E) HE staining analysis of CD8 expression in the tumor and IOD analysis (n = 3, Scale bar = 50 μm). (F) IFN-γ^+CD4$^+$ (n = 4−5 for each group). (G) Granzyme B$^+$CD4$^+$ (n = 5 for each group). (H) TNF-α^+CD4$^+$ (n = 5−6 for each group) among CD4$^+$ T cells. (I) Schematic representation of the co-culture system for macrophages and CD8$^+$ T lymphocytes. (J) ADNPs treated M2-like BMDMs reversed the proliferation of CD8$^+$ T cells and (K) the statistics. (n = 4 per group). *P < 0.05, **P < 0.01, ***P < 0.001, ****P < 0.0001. Data are presented as mean ± SEM and analyzed by one-way ANOVA.

The results showed that 1 μg/kg formononetin is unable to restrain the tumour like ADNPs or 10 mg/kg formononetin in the 4T1 murine model (Fig. S13A−S13E).

The molecular docking analysis showed that a hydrophobic bond was provided by Leu350 and Thr335. Besides, the Ile314, Ile319, Leu331, Val348, Val351, Pro352 formed π−Alkyl interactively. The mean binding energies of docking (−8 kcal/mol) in formononetin uncovered that it has a strong binding ability to human TLR2 (Fig. 8G). Furthermore, the hydrophobic surface mapping revealed that TLR2 interacts within the hydrophobic pocket of formononetin, indicating its role as a hydrophobic ligand (Supporting Information Fig. S14A). Molecular dynamics simulations further confirmed that the TLR2-formononetin complex achieved a stable conformation after 20 ns (Fig. S14B).

To further elucidate the interaction between formononetin and TLR2-mediated biological activity, a pull-down assay was employed (Fig. 8H and I), and the results of MS analysis identified TLR2 as a potential direct binding partner of formononetin (Fig. 8J and K). The interaction of TLR2 and formononetin was validated by using an immunofluorescent confocal microscope (Fig. 8L).

4. Discussion

Platinum-based drugs are widely used in chemotherapeutic agents given their proven efficacy against various malignancies, including TNBC[36]. Although platinum-based drugs have been

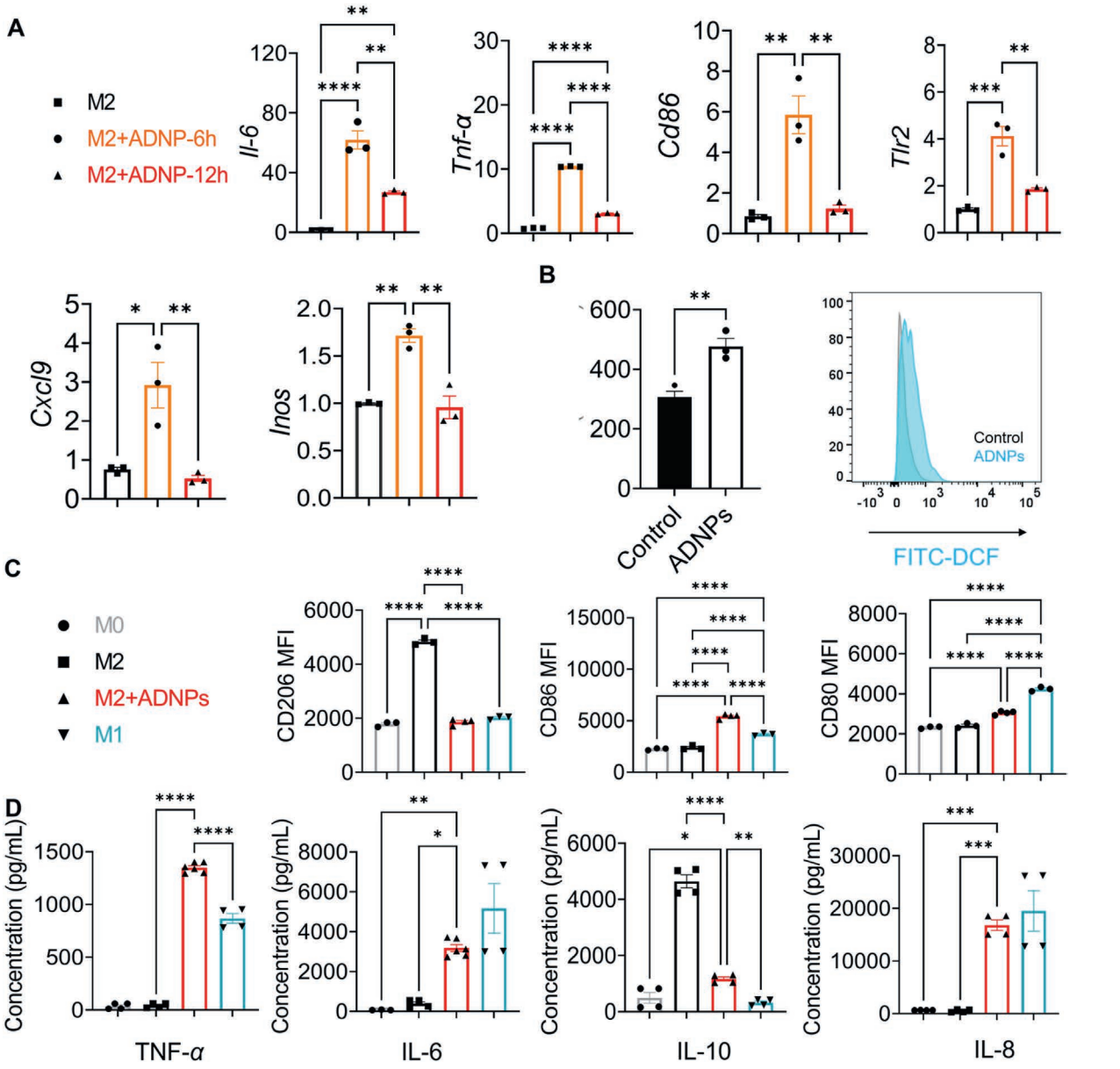

Figure 7 ADNPs reprogram M2-like macrophages into an M1-like phenotype. (A) RT-PCR analysis of *IL-6*, *tnfα*, *cxcl9*, *inos*, *tlr2*, and *cd86* mRNA expression in M2-like macrophages treated with ADNPs for 6 and 12 h *in vitro* ($n = 3$ per group). (B) ROS level in supernatants of BMDMs was detected by FACS *in vitro*. (C) Mean fluorescence intensity analysis of CD206, CD80, and CD86 of BMDMs *in vitro* ($n = 3$ per group). (D) Concentration of TNF-α, IL-6, IL-10, and IL-8 in the supernatant of BMDMs treated with ADNPs *in vitro* ($n = 3$–6 per group). $^{*}P < 0.05$, $^{**}P < 0.01$, $^{***}P < 0.001$, $^{****}P < 0.0001$. Data are presented as mean ± SEM and analyzed by one-way ANOVA or *t* test.

demonstrated to extend DFS, their function in improving the recurrence, metastasis rate, and overall survival rate in TNBC has been argued[37,38]. Additionally, platinum-based chemotherapy is often associated with systemic toxicities such as myelosuppression, peripheral blood toxicity, and chemotherapy-induced cognitive impairment[37,39], significantly hindering treatment progress due to the intolerable side effects. Therefore, improving efficacy while reducing the adverse effects of platinum-based chemotherapy is a key challenge for TNBC treatment. Currently, the role of neoadjuvant therapy has been widely investigated, underscoring its significance in reducing metastatic foci and promoting the likelihood of surgery in patients with advanced cancer. However, given the low efficacy of neoadjuvant therapy reported in early clinical trials, with a lack of well-established standards for treatment[11], it is urgent to develop combination therapies involving platinum drugs to enhance the effectiveness and safety of neoadjuvant treatment.

Our findings indicate that the TME of post-chemotherapy in TNBC is characterized by M2-TAM^{high} CD8^{+} T^{low}, a phenotype associated with poor long-term survival prognosis. Therefore, implementing a neoadjuvant chemotherapy strategy that reprograms the TME by promoting M1 polarization of TAMs while enhancing CD8^{+} T cell infiltration could significantly ameliorate the clinical outcomes of chemotherapy-based TNBC patients.

PDNPs are highly stable and bioavailable drug delivery systems and have recently been devoted to cancer research, attributed

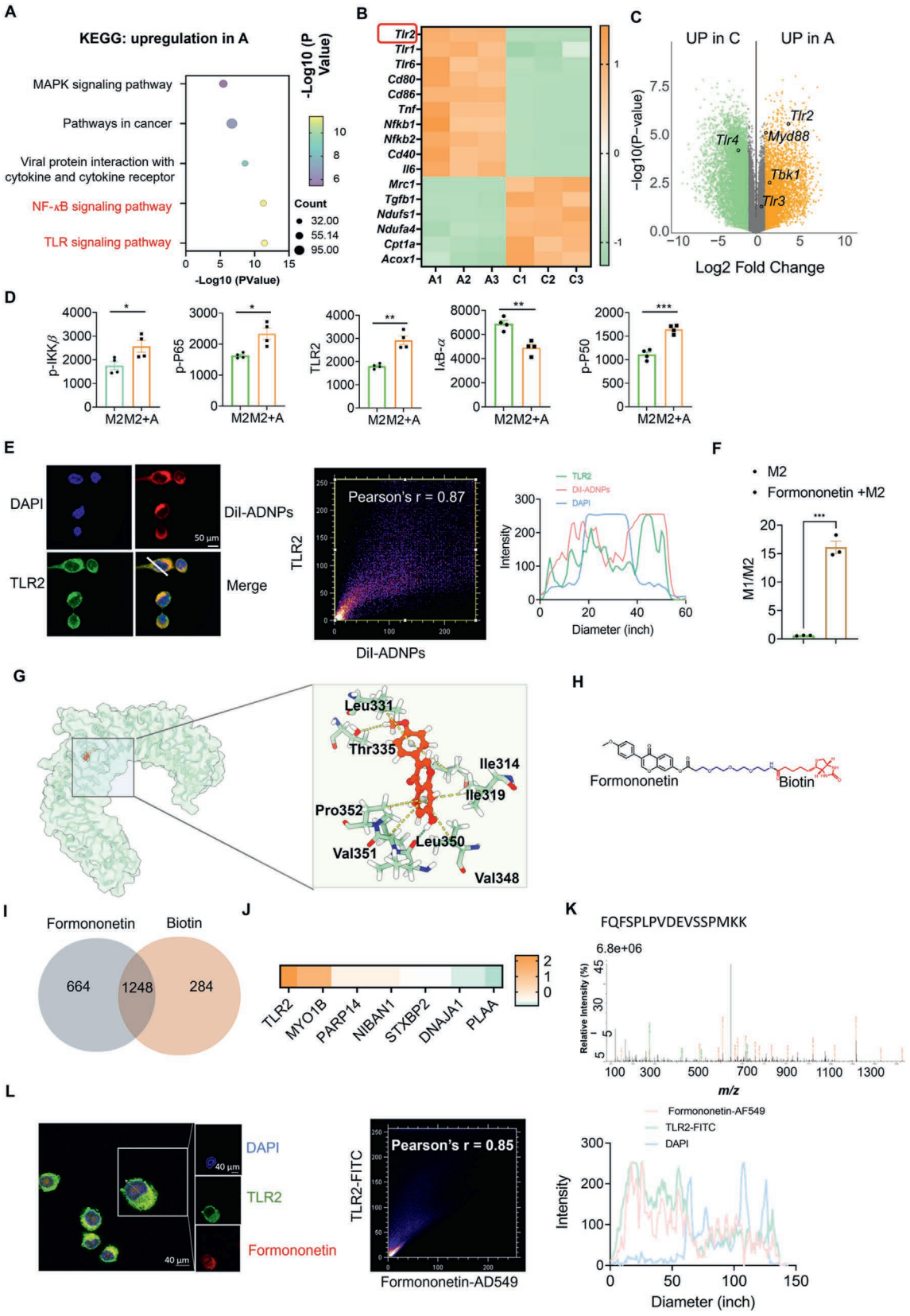

Figure 8 Active ingredient of ADNPs reprograms TAMs *via* the TLR2 pathway. (A) KEGG pathway analysis highlighting upregulated signaling pathways. (B) Heatmap of TLR-related pathway gene expression in bone marrow-derived macrophages (BMDMs). (C) Volcano plot analysis of differentially expressed genes in M2-like BMDMs treated with or without ADNPs. (D) Flow cytometry analysis of TLR2, phosphorylated IKKβ (*p*-IKKβ), phosphorylated p50 (p-P50), IκBα, and phosphorylated p65 (p-P65) protein expression. (E) Representative confocal

to their high efficiency and low toxicity[40]. The bioactivity of PDNPs varies depending on their plant source, thus providing a broad scope and potential for personalized therapies.

Recent studies have found that Astragalus plays a role in improving immune suppression by activating M1 macrophages and $CD8^+$ T cells in the TME in lung cancer[27,41]. In our study, we showed that ADNPs, extracted from Astragalus, were exosome-like nanovesicles with similar lipid components compared with other PDNPs and can be efficiently taken up by macrophages *via* macropinocytosis. Many experiments in this research demonstrated that ADNPs significantly reduced the expression of the M2-like subtype and increased the M1-like subtype percentage without changing the macrophage amount. Additionally, our experiments confirmed that ADNP-treated M2 macrophages directly enhanced the proliferation of $CD8^+$ T lymphocytes *in vitro*, which indicates thoroughly reversing the inhibitory TME after chemotherapy in TNBC.

In this study, using the combination neoadjuvant therapy regimen of ADNPs and Cisplatin, we are the first to show that ADNPs-Cis therapy significantly inhibits the tumour growth and progression in three different TNBC preclinical murine models. Furthermore, our study confirmed that ADNPs-Cis therapy effectively modulated macrophage polarization and enhanced the therapeutic effect of Cisplatin. The anti-tumour efficacy of the ADNPs-Cis therapy in TNBC lacking macrophages was markedly reduced, indicating that macrophages play a pivotal role in the ADNPs-Cis-mediated treatment. Both tail vein injection and intraperitoneal injection are well-established *in vivo* administration methods commonly used in basic research. In the current study, intraperitoneal injection was selected based on the hypothesis that the abundance of macrophages in the peritoneal cavity may enhance drug absorption.

We also observed that ADNPs significantly promoted the infiltration and proliferation of $CD8^+$ T lymphocytes in the tumour, accompanied by the increased secretion of multiple cytotoxic inflammatory factors like IFN-γ, Granzyme B, and TNF-α compared with the Cis group. Besides, ADNPs and ADNPs-Cis groups significantly promoted the multiple cytotoxic inflammatory factors in $CD4^+$ T cells compared with the Cis group. These data indicated that the ADNPs and ADNP-CIS appear to boost macrophage antigen presentation, leading to enhanced T cell activity, aligning with the CFSE proliferation assay results (Fig. 6J).

Besides, ADNPs are phagocytosed into macrophages at the 6-h time point and activate the TLR2 signaling pathway, which induces cytokine secretion. As ADNPs depend on macropinocytosis to be phagocytosed into macrophages, and the stimulated cells exhibit initial gene expression fluctuations, following regulatory networks enforce decay kinetics to limit prolonged deviations[1]. Conversely, control populations sustain higher steady-state expression, with compensatory repression mechanisms likely constraining maximal transcriptional output. Cells employ negative feedback loops to restore transcriptional homeostasis post-stimulation[2]. Thus, the gene expression change of Toll-like signaling decreases in 12 h compared with the 6 h point expression.

Compared to cisplatin monotherapy, the ADNPs-Cis treatment significantly inhibited the expression of co-inhibitory molecules in T lymphocytes in the tumour, further demonstrating that ADNPs-Cis could reverse the immunosuppressive TME and reactive adaptive immune system to defend against tumour progression. Thus, reversing the inhibitory tumour immune condition is the key breakthrough for ADNPs-Cis combined with traditional chemotherapy.

The metastasis can result in high mortality rates among TNBC patients. The activation of anti-tumour immune response along with powerful tumour immune memory is a necessary condition to combat tumour recurrence and tumour metastasis[42]. We found that ADNPs-Cis significantly triggered more durable anti-tumour immune memory, effectively inhibiting tumour metastasis in both the lung and liver in the TNBC murine model. As liver metastasis and lung metastasis are both important tumour progression in TNBC clinical treatment, the ADNPs-Cis treatment group showed minimal metastasis compared with Cisplatin alone, which brings a promising combination treatment scheme.

The toxicity of platinum-based therapy severely reduces the quality of life and adherence for TNBC patients. For example, myelosuppression is one of the main side effects of traditional chemotherapy, resulting in a reduction in red blood cell and platelet counts. Although the aforementioned PDNPs all exhibited great safety *in vivo*, the improvement of haematological toxicity induced by chemotherapy was not reported before. Previous studies have shown that Astragalus can effectively mitigate myelosuppression and promote haematopoiesis[43]. Our experimental results revealed that compared with the Cisplatin treatment group, ADNPs and ADNPs-Cis therapy significantly alleviated the myelosuppression caused by Cisplatin. Recently, a new targeted therapy, Sacituzumab Govitecan, has been applied in a metastatic TNBC II/III clinical trial. However, 85% patients suffered side effects like myelosuppression, anaemia, diarrhea, etc., and these impede the future clinical research[44]. The haematological toxicities have severely hindered the cancer treatment, neither chemotherapy nor genetically engineered CAR-T therapy[45]. Numerous PDNPs have been reported with great anti-tumor efficiency, such as ginseng, tea leaves, tea flower (TFEN)[46], grapefruit, and melon, etc[47]. Researchers have found that the miRNA, protein, and lipid all play important roles in the biofunction of PDNPs, and the lipids have attracted much attention recently[48]. Results of our team showed that both GDNPs and ADNPs could inhibit TNBC by targeting and polarizing TAMs. Notably, the ADNPs showed enhanced efficiency compared with previously reported GDNPs in the 4T1 murine breast cancer model. The ADNP is a TLR2-specific agonist, while GDNP was reported as a natural TLR4 agonist (Supporting Information Fig. S15). We hypothesized that the difference in lipid composition may affect the biofunction of PDNPs, especially targeting the immune

microscopy images showing co-localization of TLR2 and DiI-labeled ADNPs in BMDMs. Fluorescence co-localization and Pearson correlation coefficient analysis were performed. (F) Flow cytometry analysis of M2-like BMDMs polarization following formononetin treatment. (G) Molecular docking of formononetin with TLR2. (H) Structure of biotin-linked formononetin. (I) Proteins identified in pull-down and mass spectrometry (MS) assays using formononetin-biotin. (J) Selected proteins identified by MS that interact with formononetin-biotin. (K) MS identification of TLR2 protein. $*P < 0.05$, $***P < 0.001$. ($n = 3$ per group). (L) Representative confocal microscopy images showing co-localization of formononetin and TLR2 in BMDMs. Fluorescence co-localization and Pearson correlation coefficient analyses were performed. Scale bar = 100 μm. Data are presented as mean ± SEM and analyzed by one-way ANOVA or *t* test.

cells[49−51]. Briefly, GDNPs were reported with a high amount of digalactosyl monoacylglycerol (DGMG, 59.4%), phosphatidyl ethanolamine (PE, 16.8%), and ceramide (Cer, 13.8%). The top three lipids in ADNPs are sphingolipid (SPH, 92.9%), ceramides (Cer, 4.2%), and triglyceride (TG, 0.6%). Notably, the GDNPs showed much higher amounts of Cer compared with those in ADNPs (Cer in GDNPs *vs* ADNPs: 13.8% *vs* 4.2%). The C6-Cer has been reported as a powerful liver tumor suppressor by activating TLR4 in TAMs[52]. In comparison, the formononetin was featured as the main ingredient in ADNPs for activation of TLR2 in TAMs. Besides, the lipids' composition was reported with an adjustable capacity of drug transmembrane transportation, which is consistent with previous reports[24]. We found that the level of SPH in ADNPs is similar to that of the general cell membrane, which is important in the adjustment of lipid raft construction. Since TFEN was reported to have direct destruction of tumors rather than modulation of TAMs. The lipidomic results revealed that phosphatidylcholine (PC, ∼26.6%), triglyceride (TG, ∼23.4%), and phosphatidyl-ethanolamine (PE, ∼15.2%) were the major lipid compositions of TFENs. Apart from the similar PE levels in GDNPs and TFENs, remarkable Cer was not reported in TFEN. Although TFEN is rich in polyphenols and flavonoids, compounds that have been identified as direct anti-tumor agents[46], the precise chemical entities have yet to be fully elucidated.

To further understand the mechanisms of ADNPs in macrophage polarization, we conducted RNA-seq analysis on M2-BMDMs treated with ADNPs. The results showed that ADNPs mimic the simple feature of plant immune defence and could specifically activate TLR. Compared with other TLR mRNA expression, TLR2 showed higher distinction in macrophage RNA-sequence analysis, which indicates ADNPs are the preferred agonist of TLR2 for targeting macrophages. Numerous studies have demonstrated that TLR2 agonists showed great capability in tumour inhibition, anti-influenza virus infection, and improving organ development[53]. Thus, developing TLR2 agonists with a great dosage form and drug design may promote clinical application progression in the future. Multiple TLR agonists have been reported, including LPS, MPLA, Pam3CSK4, and Poly(I:C). For LPS, the type of microbes it derives from can affect its specificity[54]. Also, research showed that the established TLR agonists exerted high toxicity[21]. Possibly due to the consequence of the nonspecific activation of cell receptors and the unwanted expression of cytokine storm[55,56]. Unlike previously reported TLR2 agonists, the acGM1.8, which often relies on complex synthesis, ADNPs are edible with simple preparation methodology, but continually engage in the plant host defense process, thus exhibiting remarkable effects of TLR2 agonist without sacrificing bio-compatibility and security (for example, haematological toxicity) *in vivo*[21].

Given the multiple components present in ADNPs, it is critical to explore the active compound responsible for its effect on macrophages. Through testing the macrophage polarization capabilities of the major components in ADNPs, we discovered that formononetin is the primary active compound in macrophage polarization. Formononetin, a lipophilic phytoestrogen, has been demonstrated in multiple studies to exhibit potent anti-tumor activity across various tumour models[35]. Due to its crystalline form, poor water solubility, and lipid solubility, formononetin is limited in the fields of medicine and the food field[57]. Our findings demonstrate that ADNPs can be applied as a natural carrier for formononetin at low concentration, which triggers anti-tumour immune responses. This study is the first to reveal the activation effects of formononetin on macrophages. Furthermore, using pull-down and mass spectrum techniques, we analysed the binding site of formononetin in the macrophage and conducted preliminary validation through molecular docking and confocal immunofluorescence. As formononetin is characterized by low water solubility, it is preferred to be assembled near the membrane of ADNPs. When ADNPs move close to the macrophage, the formononetin on the membrane combines with TLR2. When the cytoskeleton changed, the membrane of the macrophage stretched out, and the micropinocytosis could engulf the ADNPs into the macrophage. With the formononetin-related transmembrane material conduction, the signal transduction begins even with minimal ATP consumption (Supporting Information Fig. S16). After that, the membrane disturbance enhances the communication of formononetin inside ADNPs with more TLR2 protein on macrophages. Although the high dose formononetin could suppress the 4T1 tumour without obvious difference compared with the ADNPs treatment, the low water solubility limited the clinical application. Further analysis using mass spectrometry and macrophage polarization *in vitro* assays confirmed that the minimal concentration of formononetin in macrophage polarization is 50 times higher than the concentration of formononetin in ADNPs under which M2-like macrophages polarized, indicating the importance of the nano construction of ADNPs, rather than formononetin alone. Further research should focus on the anti-tumor activity of ADNPs combined with different chemotherapy-based drugs and related clinical studies. The mechanism of ADNPs composition in reversing the haematological toxicities caused by chemotherapy still needs to be investigated in the future. More clearly, the pharmacological function of ADNPs *in vivo*, especially the mechanism of reversing myelosuppression, is indispensable to be uncovered. Furthermore, the therapeutic efficacy and pharmacological mechanisms of ADNPs administered *via* oral delivery and tail vein injection for various diseases will be explored in future studies.

5. Conclusions

In this study, we purified ADNPs that showed a great phenotype to polarize TAMs and restore the anti-tumor immune system. Moreover, ADNPs, as the ideal TLR2 agonist with low toxicity and high specificity, could better enhance the chemotherapy treatment in the 4T1 TNBC murine model. The proposed ADNPs-Cis regimenis a novel neoadjuvant therapy with high therapeutic efficacy and low myelosuppression. These follow-up studies will help validate the clinical potential of ADNPs, providing additional scientific evidence and therapeutic options for TNBC treatment. The combined treatment of ADNPs and Cisplatin successfully provides a new avenue for highly efficient neoadjuvant immunochemotherapy.

Acknowledgements

We extend our sincere gratitude to Prof. Binzhi Qian (Fudan University, China), Dr. Rongling Wang (Charité - Universitätsmedizin Berlin, Max Rubner Center, Germany), Dr. Ruoyu Ma (Fudan University, China), Prof. Laifa Shen (Nanjing University of Aeronautics and Astronautics), and Dr. Wenjie Huang (Nanjing University of Chinese Medicine) for their invaluable insights and critical review of this manuscript. This research was supported by funding from the National Natural

Science Foundation of China (Grants Nos. 82204696, 82125037, 82305052, and 82402052), the National Key R&D Program of China (Grant Nos. 2024YFA1209900 and 2024YFA1209901), the Young Elite Scientists Sponsorship Program by CAST (2022-QNRC1-04, China), and Nanjing University of Chinese Medicine (Grant No. XPT 82204696, China).

Author contributions

Xuan Han, Yongbing Yang, and Jing Chen jointly conceived, designed, and co-authored the study. Data acquisition was carried out by Xuan Han, Yongbing Yang, Qiwen Lu, Zihan Zhang, Chengcheng Zhang, Xi Wang, Yueyi Huang, Hurong Shen and Qichen Zhan. All authors participated in data analysis, result interpretation, manuscript revision, and final approval. Funding acquisition and overall supervision of the project were managed by Xuan Han, Yongbing Yang, and Peng Cao. All of the authors have read and approved the final manuscript.

Conflicts of interest

The authors declare no competing financial or personal interests that could influence the work reported in this paper.

Appendix A. Supporting information

Supporting information to this article can be found online at https://doi.org/10.1016/j.apsb.2026.03.051.

References

1. Karim AM, Eun Kwon J, Ali T, Jang J, Ullah I, Lee YG, et al. Triple-negative breast cancer: epidemiology, molecular mechanisms, and modern vaccine-based treatment strategies. *Biochem Pharmacol* 2023; **212**:115545.
2. Yin L, Duan JJ, Bian XW, Yu SC. Triple-negative breast cancer molecular subtyping and treatment progress. *Breast Cancer Res* 2020;**22**: 61.
3. Wu SY, Wang H, Shao ZM, Jiang YZ. Triple-negative breast cancer: new treatment strategies in the era of precision medicine. *Sci China Life Sci* 2021;**64**:372−88.
4. da Silva JL, Cardoso Nunes NC, Izetti P, de Mesquita GG, de Melo AC. Triple negative breast cancer: a thorough review of biomarkers. *Crit Rev Oncol Hematol* 2020;**145**:102855.
5. Korde LA, Somerfield MR, Carey LA, Crews JR, Denduluri N, Hwang ES, et al. Neoadjuvant chemotherapy, endocrine therapy, and targeted therapy for breast cancer: ASCO guideline. *J Clin Oncol* 2021;**39**:1485−505.
6. Chatila WK, Kim JK, Walch H, Marco MR, Chen CT, Wu F, et al. Genomic and transcriptomic determinants of response to neoadjuvant therapy in rectal cancer. *Nat Med* 2022;**28**:1646−55.
7. (EBCTCG) EBCTCG. Long-term outcomes for neoadjuvant versus adjuvant chemotherapy in early breast cancer: meta-analysis of individual patient data from ten randomised trials. *Lancet Oncol* 2018;**19**: 27−39.
8. Liedtke C, Mazouni C, Hess KR, André F, Tordai A, Mejia JA, et al. Response to neoadjuvant therapy and long-term survival in patients with triple-negative breast cancer. *Clin Oncol* 2023;**41**: 1809−15.
9. Mason SR, Willson ML, Egger SJ, Beith J, Dear RF, Goodwin A. Platinum chemotherapy for early triple-negative breast cancer. *Breast* 2024;**75**:103712.
10. van den Ende NS, Nguyen AH, Jager A, Kok M, Debets R, van Deurzen CHM. Triple-negative breast cancer and predictive markers of response to neoadjuvant chemotherapy: a systematic review. *Int J Mol Sci* 2023;**24**:2969.
11. Leon-Ferre RA, Goetz MP. Advances in systemic therapies for triple-negative breast cancer. *BMJ* 2023;**381**:e071674.
12. Deepak KGK, Vempati R, Nagaraju GP, Dasari VR, SN, Rao DN, et al. Tumor microenvironment: challenges and opportunities in targeting metastasis of triple negative breast cancer. *Pharmacol Res* 2020;**153**:104683.
13. Li H, Yang P, Wang J, Zhang J, Ma Q, Jiang Y, et al. HLF regulates ferroptosis, development, and chemoresistance of triple-negative breast cancer by activating tumor cell−macrophage crosstalk. *J Hematol Oncol* 2022;**15**:2.
14. Xiang X, Wang J, Lu D, Xu X. Targeting tumor-associated macrophages to synergize tumor immunotherapy. *Signal Transduct Targeted Ther* 2021;**6**:75.
15. van Elsas MJ, Middelburg J, Labrie C, Roelands J, Schaap G, Sluijter M, et al. Immunotherapy-activated T cells recruit and skew late-stage activated M1-like macrophages that are critical for therapeutic efficacy. *Cancer Cell* 2024;**42**:1032-50.e10.
16. Pan Y, Yu Y, Wang X, Zhang T. Tumor-associated macrophages in tumor immunity. *Front Immunol* 2020;**11**:583084.
17. Kumari N, Choi SH. Tumor-associated macrophages in cancer: recent advancements in cancer nanoimmunotherapies. *J Exp Clin Cancer Res* 2022;**41**:68.
18. Li C, Xu X, Wei S, Jiang P, Xue L, Wang J. Tumor-associated macrophages: potential therapeutic strategies and future prospects in cancer. *J Immunother Cancer* 2021;**9**:e001341.
19. Krutzik SR, Tan B, Li H, Ochoa MT, Liu PT, Sharfstein SE, et al. TLR activation triggers the rapid differentiation of monocytes into macrophages and dendritic cells. *Nat Med* 2005;**11**:653−60.
20. Cheng K, Wang X, Zhang S, Yin H. Discovery of small-molecule inhibitors of the TLR1/TLR2 complex. *Angew Chem Int Ed Engl* 2012;**51**:12246−9.
21. Feng Y, Mu R, Wang Z, Xing P, Zhang J, Dong L, et al. A toll-like receptor agonist mimicking microbial signal to generate tumor-suppressive macrophages. *Nat Commun* 2019;**10**:2272.
22. He B, Cai Q, Qiao L, Huang CY, Wang S, Miao W, et al. RNA-binding proteins contribute to small RNA loading in plant extracellular vesicles. *Nat Plants* 2021;**7**:342−52.
23. Cai Q, Qiao L, Wang M, He B, Lin FM, Palmquist J, et al. Plants send small RNAs in extracellular vesicles to fungal pathogens to silence virulence genes. *Science* 2018;**360**:1126−9.
24. Cao M, Yan H, Han X, Weng L, Wei Q, Sun X, et al. Ginseng-derived nanoparticles alter macrophage polarization to inhibit melanoma growth. *J Immunother Cancer* 2019;**7**:326.
25. Han X, Wei Q, Lv Y, Weng L, Huang H, Wei Q, et al. Ginseng-derived nanoparticles potentiate immune checkpoint antibody efficacy by reprogramming the cold tumor microenvironment. *Mol Ther* 2022;**30**: 327−40.
26. Liang J, Yang C, Li P, Zhang M, Xie X, Xie X, et al. Astragaloside IV inhibits AOM/DSS-induced colitis-associated tumorigenesis *via* activation of PPARγ signaling in mice. *Phytomedicine* 2023;**121**:155116.
27. Li S, Sun Y, Huang J, Wang B, Gong Y, Fang Y, et al. Anti-tumor effects and mechanisms of *Astragalus membranaceus* (AM) and its specific immunopotentiation: status and prospect. *J Ethnopharmacol* 2020;**258**:112797.
28. Li W, Hu X, Wang S, Jiao Z, Sun T, Liu T, et al. Characterization and anti-tumor bioactivity of astragalus polysaccharides by immunomodulation. *Int J Biol Macromol* 2020;**145**:985−97.
29. Xu H, Zhou Y, Lei T. Volatile analysis in fresh and dried *Astragali Radix*. *Food Sci (N Y)* 2011;**32**:171−4.
30. Elabd H, Wang HP, Shaheen A, Matter A. *Astragalus membranaceus* nanoparticles markedly improve immune and anti-oxidative responses; and protection against *Aeromonas veronii* in Nile tilapia *Oreochromis niloticus*. *Fish Shellfish Immunol* 2020;**97**:248−56.
31. Cong M, Tan S, Li S, Gao L, Huang L, Zhang HG, et al. Technology insight: Plant-derived vesicles-how far from the clinical biotherapeutics and therapeutic drug carriers?. *Adv Drug Deliv Rev* 2022;**182**:114108.

32. Sipos O, Tovey H, Quist J, Haider S, Nowinski S, Gazinska P, et al. Assessment of structural chromosomal instability phenotypes as biomarkers of carboplatin response in triple negative breast cancer: the TNT trial. *Ann Oncol* 2021;**32**:58−65.
33. Arora S, Kumar A, Batra A. Effect of adjuvant paclitaxel and carboplatin on survival in early triple-negative breast cancer. *JAMA Oncol* 2021;**7**:460−1.
34. Basak U, Sarkar T, Mukherjee S, Chakraborty S, Dutta A, Dutta S, et al. Tumor-associated macrophages: an effective player of the tumor microenvironment. *Front Immunol* 2023;**14**:1295257.
35. Aliya S, Alhammadi M, Park U, Tiwari JN, Lee JH, Han YK, et al. The potential role of formononetin in cancer treatment: an updated review. *Biomed Pharmacother* 2023;**168**:115811.
36. Zhang C, Xu C, Gao X, Yao Q. Platinum-based drugs for cancer therapy and anti-tumor strategies. *Theranostics* 2022;**12**:2115−32.
37. Romani AMP. Cisplatin in cancer treatment. *Biochem Pharmacol* 2022;**206**:115323.
38. Saleh RR, Nadler MB, Desnoyers A, Meti N, Fazelzad R, Amir E. Platinum-based chemotherapy in early-stage triple negative breast cancer: a meta-analysis. *Cancer Treat Rev* 2021;**100**:102283.
39. Oun R, Moussa YE, Wheate NJ. The side effects of platinum-based chemotherapy drugs: a review for chemists. *Dalton Trans* 2018;**47**:6645−53.
40. Li A, Li D, Gu Y, Liu R, Tang X, Zhao Y, et al. Plant-derived nanovesicles: further exploration of biomedical function and application potential. *Acta Pharm Sin B* 2023;**13**:3300−20.
41. Yu WD, Sun G, Li J, Xu J, Wang X. Mechanisms and therapeutic potentials of cancer immunotherapy in combination with radiotherapy and/or chemotherapy. *Cancer Lett* 2019;**452**:66−70.
42. Han J, Khatwani N, Searles TG, Turk MJ, Angeles CV. Memory $CD8^+$ T cell responses to cancer. *Semin Immunol* 2020;**49**:101435.
43. Nian Q, Liu R, Zeng J. Unraveling the pathogenesis of myelosuppression and therapeutic potential of natural products. *Phytomedicine* 2024;**132**:155810.
44. Bardia A, Hurvitz SA, Tolaney SM, Loirat D, Punie K, Oliveira M, et al. Sacituzumab Govitecan in metastatic triple-negative breast cancer. *N Engl J Med* 2021;**384**:1529−41.
45. Rejeski K, Jain MD, Shah NN, Perales MA, Subklewe M. Immune effector cell-associated haematotoxicity after CAR T-cell therapy: from mechanism to management. *Lancet Haematol* 2024;**11**:e459−70.
46. Chen Q, Li Q, Liang Y, Zu M, Chen N, Canup BSB, et al. Natural exosome-like nanovesicles from edible tea flowers suppress metastatic breast cancer *via* ROS generation and microbiota modulation. *Acta Pharm Sin B* 2022;**2**:907−23.
47. Feng J, Xiu Q, Huang Y, Troyer Z, Li B, Zheng L. Plant-derived vesicle-like nanoparticles as promising biotherapeutic tools: present and future. *Adv Mater* 2023 Jun;**35**:e2207826.
48. Li S, Zhang R, Wang A, Li Y, Zhang M, Kim J, et al. *Panax notoginseng*: derived exosome-like nanoparticles attenuate ischemia−reperfusion injury *via* altering microglia polarization. *J Nanobiotechnol* 2023;**1**:416.
49. Suzuki Y, Yakuwa M, Sato M, Samaridou E, Beck-Broichsitter M, Maeki M, et al. Splenic B cell-targeting lipid nanoparticles for safe and effective mRNA vaccine delivery. *J Control Release* 2025;**382**:113687.
50. Chen SP, Blakney AK. Immune response to the components of lipid nanoparticles for ribonucleic acid therapeutics. *Curr Opin Biotechnol* 2024;**85**:103049.
51. Karyu H, Niki T, Sorimachi Y, Hata S, Shimabukuro-Demoto S, Hirabayashi T, et al. Collaboration between a *cis*-interacting natural killer cell receptor and membrane sphingolipid is critical for the phagocyte function. *Front Immunol* 2024;**15**:1401294.
52. Li G, Liu D, Kimchi ET, Kaifi JT, Qi X, Manjunath Y, et al. Nanoliposome C6-Ceramide increases the anti-tumor immune response and slows growth of liver tumors in mice. *Gastroenterology* 2018;**4**:1024−36.
53. Liu X, Liu L, Ren Z, Yang K, Xu H, Luan Y, et al. Dual targeting of innate and adaptive checkpoints on tumor cells limits immune evasion. *Cell Rep* 2018;**24**:2101−11.
54. Werling D, Jann OC, Offord V, Glass EJ, Coffey TJ. Variation matters: TLR structure and species-specific pathogen recognition. *Trends Immunol* 2009;**30**:124−30.
55. Li Y, Shi Y, McCaw L, Li YJ, Zhu F, Gorczynski R, et al. Microenvironmental interleukin-6 suppresses toll-like receptor signaling in human leukemia cells through miR-17/19A. *Blood* 2015;**126**:766−78.
56. Kim S, Takahashi H, Lin WW, Descargues P, Grivennikov S, Kim Y, et al. Carcinoma-produced factors activate myeloid cells through TLR2 to stimulate metastasis. *Nature* 2009;**457**:102−6.
57. Guo BH, Xu DQ, Liu XH, Liao CC, Li SB, Huang ZX, et al. Characterization and cytotoxicity of PLGA nanoparticles loaded with formononetin cyclodextrin complex. *Drug Deliv Sci Tec* 2017;**41**:375−83.